U.S. Department
of Transportation
Federal Railroad
Administration

Office of Research,
Development and Technology
Washington, DC 20590

Rail Safety Improvement Through Enhanced Understanding of Ballast and Subgrade Interactions

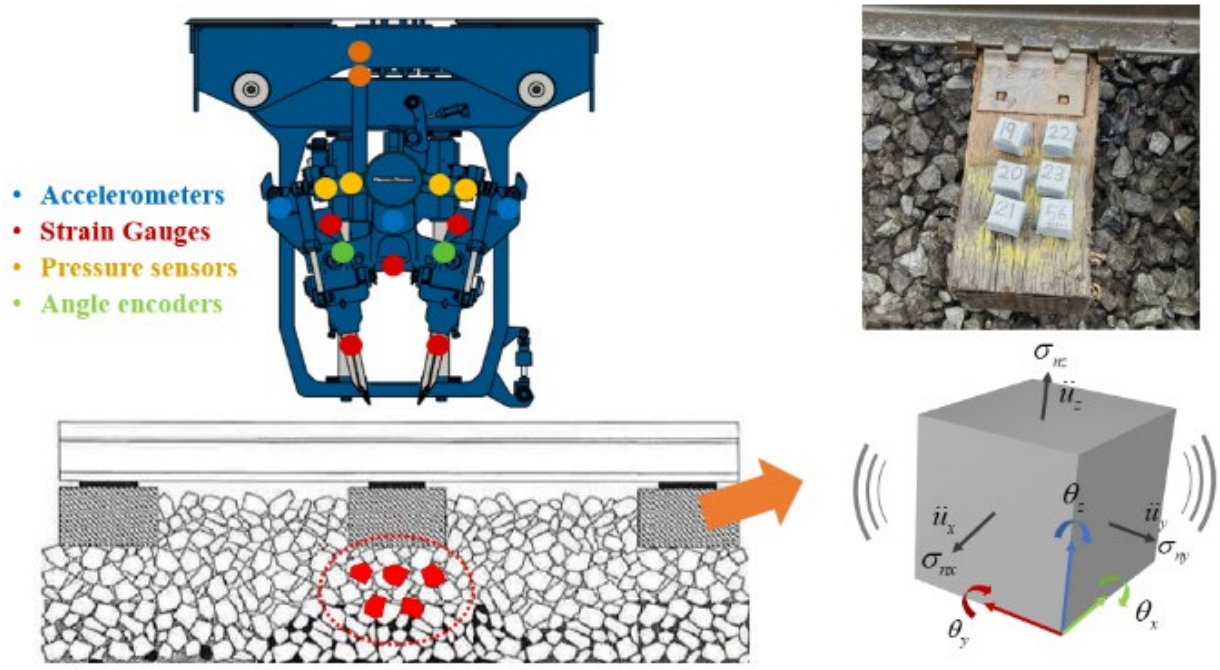

DOT/FRA/ORD-26/04

Final Report | April 2026

REPORT DOCUMENTATION PAGE

Form Approved
OMB No. 0704-0188

1. REPORT DATE *(DD-MM-YYYY)*	**2. REPORT TYPE**	**3. DATES COVERED** *(From - To)*
7 April 2026	Technical Report	April 2021 – April 2023

4. TITLE AND SUBTITLE
Rail Safety Improvement through Enhanced Understanding of Ballast and Subgrade Interactions

5a. CONTRACT NUMBER

5b. GRANT NUMBER

5c. PROGRAM ELEMENT NUMBER

6. AUTHOR(S)
Hai Huang – ORCiD: 0000-0002-0023-2915
Yuliang Zhou – ORCiD: 0000-0002-7424-031X

5d. PROJECT NUMBER

5e. TASK NUMBER

5f. WORK UNIT NUMBER

7. PERFORMING ORGANIZATION NAME(S) AND ADDRESS(ES)
Penn State Altoona
3000 Ivyside Park
Altoona, PA 16601

8. PERFORMING ORGANIZATION REPORT NUMBER

9. SPONSORING/MONITORING AGENCY NAME(S) AND ADDRESS(ES)
U.S. Department of Transportation
Federal Railroad Administration
Office of Research, Development, and Technology
Washington, DC 20590

10. SPONSOR/MONITOR'S ACRONYM(S)

11. SPONSOR/MONITOR'S REPORT NUMBER(S)
DOT/FRA/ORD-26/04

12. DISTRIBUTION/AVAILABILITY STATEMENT
This document is available to the public through the FRA website.

13. SUPPLEMENTARY NOTES
COR:

14. ABSTRACT
Between April 2021 and April 2023, the Federal Railroad Administration sponsored a research team from The Pennsylvania State University to conduct a study on optimizing tamping maintenance. In this report, researchers examine the impact of various tamping parameters on railway ballast performance. Field tests were conducted on Norfolk Southern Railway's mainline at Bellwood and Tunnelhill in Pennsylvania, as well as Chesapeake, Virginia. Using data collected from SmartRock sensors embedded in the ballast, the team analyzed movement and stress changes to establish the relationship between ballast performance and tamping behavior. Additionally, an energy analysis revealed that the energy absorbed by the ballast is a reliable indicator for assessing ballast stability. The findings in this report offer valuable insights for tamping operators to optimize tamping parameters, which in turn can enhance track safety and reliability. By refining tamping practices, railway operators can improve operational efficiency and reduce maintenance costs, contributing to safer and more cost-effective railway operations.

15. SUBJECT TERMS
Railroad tamping, ballast performance, track stability, tamping parameters, SmartRock sensors

16. SECURITY CLASSIFICATION OF:			**17. LIMITATION OF ABSTRACT**	**18. NUMBER OF PAGES**	**19a. NAME OF RESPONSIBLE PERSON**
a. REPORT	**b. ABSTRACT**	**c. THIS PAGE**			**19b. TELEPHONE NUMBER** *(Include area code)*
Unclassified	Unclassified	Unclassified		44	

Standard Form 298 (Rev. 8/98)
Prescribed by ANSI Std. Z39.18

METRIC/ENGLISH CONVERSION FACTORS

ENGLISH TO METRIC	METRIC TO ENGLISH
LENGTH (APPROXIMATE)	**LENGTH (APPROXIMATE)**
1 inch (in) = 2.5 centimeters (cm)	1 millimeter (mm) = 0.04 inch (in)
1 foot (ft) = 30 centimeters (cm)	1 centimeter (cm) = 0.4 inch (in)
1 yard (yd) = 0.9 meter (m)	1 meter (m) = 3.3 feet (ft)
1 mile (mi) = 1.6 kilometers (km)	1 meter (m) = 1.1 yards (yd)
	1 kilometer (km) = 0.6 mile (mi)
AREA (APPROXIMATE)	**AREA (APPROXIMATE)**
1 square inch (sq in, in^2) = 6.5 square centimeters (cm^2)	1 square centimeter (cm^2) = 0.16 square inch (sq in, in^2)
1 square foot (sq ft, ft^2) = 0.09 square meter (m^2)	1 square meter (m^2) = 1.2 square yards (sq yd, yd^2)
1 square yard (sq yd, yd^2) = 0.8 square meter (m^2)	1 square kilometer (km^2) = 0.4 square mile (sq mi, mi^2)
1 square mile (sq mi, mi^2) = 2.6 square kilometers (km^2)	10,000 square meters (m^2) = 1 hectare (ha) = 2.5 acres
1 acre = 0.4 hectare (he) = 4,000 square meters (m^2)	
MASS - WEIGHT (APPROXIMATE)	**MASS - WEIGHT (APPROXIMATE)**
1 ounce (oz) = 28 grams (gm)	1 gram (gm) = 0.036 ounce (oz)
1 pound (lb) = 0.45 kilogram (kg)	1 kilogram (kg) = 2.2 pounds (lb)
1 short ton = 2,000 pounds (lb) = 0.9 tonne (t)	1 tonne (t) = 1,000 kilograms (kg) = 1.1 short tons
VOLUME (APPROXIMATE)	**VOLUME (APPROXIMATE)**
1 teaspoon (tsp) = 5 milliliters (ml)	1 milliliter (ml) = 0.03 fluid ounce (fl oz)
1 tablespoon (tbsp) = 15 milliliters (ml)	1 liter (l) = 2.1 pints (pt)
1 fluid ounce (fl oz) = 30 milliliters (ml)	1 liter (l) = 1.06 quarts (qt)
1 cup (c) = 0.24 liter (l)	1 liter (l) = 0.26 gallon (gal)
1 pint (pt) = 0.47 liter (l)	
1 quart (qt) = 0.96 liter (l)	
1 gallon (gal) = 3.8 liters (l)	
1 cubic foot (cu ft, ft^3) = 0.03 cubic meter (m^3)	1 cubic meter (m^3) = 36 cubic feet (cu ft, ft^3)
1 cubic yard (cu yd, yd^3) = 0.76 cubic meter (m^3)	1 cubic meter (m^3) = 1.3 cubic yards (cu yd, yd^3)
TEMPERATURE (EXACT)	**TEMPERATURE (EXACT)**
[(x-32)(5/9)] °F = y °C	[(9/5) y + 32] °C = x °F

QUICK INCH - CENTIMETER LENGTH CONVERSION

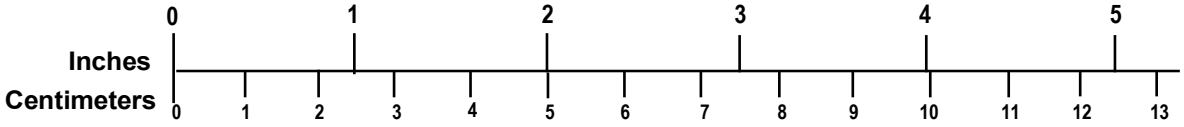

QUICK FAHRENHEIT - CELSIUS TEMPERATURE CONVERSIO

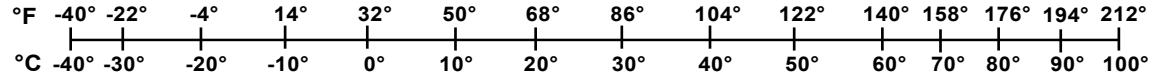

For more exact and or other conversion factors, see NIST Miscellaneous Publication 286, Units of Weights and Measures. Price $2.50 SD Catalog No. C13 10286

Updated 6/17/98

Acknowledgements

The authors thank Mr. Hugh Tompson from FRA and Dr. Ted Sussmann from the Volpe Center for their invaluable insights and guidance, and gratefully acknowledge Norfolk Southern Railway for providing access to field test sections, facilitating site organization, and assisting with the installation and monitoring of field instrumentation. The research team also extends thanks to Plasser American for supplying the testing equipment.

Contents

Illustrations

Tables

Executive Summary

The Federal Railroad Administration (FRA) sponsored a team from Pennsylvania State University Altoona to assess the performance of ballast under different tamping conditions, with a particular focus on tamping parameters. In this study, conducted between 2021 and 2023 on Norfolk Southern (NS) railway lines, the team used SmartRock sensors embedded beneath railway ties to capture real-time data on ballast particle movement, acceleration, and stress during tamping operations. These battery-powered wireless sensors were integrated into a sophisticated data acquisition (DAQ) system, providing high-frequency measurements that allow deep insights into the behavior of ballast during various tamping scenarios.

The team monitored clean and fouled ballast conditions during field tests conducted at Bellwood, PA, Tunnelhill, PA, and Chesapeake, VA. The results revealed that clean ballast responded more favorably to tamping, exhibiting effective compaction and stability with relatively consistent outcomes, particularly when subjected to longer squeezing times and multiple insertions. SmartRock sensors showed that the particles in clean ballast experienced significant reorientation and compaction during tamping, with higher accelerations recorded during the squeezing phase, leading to improved track stability.

In contrast, the fouled ballast at the Tunnelhill site demonstrated higher resistance to tamping forces, with the data showing greater acceleration peaks and less uniform compaction. The presence of fouling materials (e.g., dirt and debris) disrupted the ballast's ability to rearrange effectively, resulting in less efficient tamping and increased variability in track performance. These findings were supported by the sensor data, which highlighted the need for adjusted tamping strategies when dealing with fouled ballast, as conventional tamping approaches were less effective.

The field results also indicated that longer squeezing times and multiple insertions improved ballast compaction in clean ballast, while fouled ballast required more force and effort to achieve similar results. In addition to recording movement and stress, the SmartRock sensors provided valuable data on the energy received during tamping, which directly correlated with the effectiveness of the compaction process. In clean ballast, the energy applied during tamping was primarily used to compact the ballast particles, leading to a more stable and resilient track. However, in fouled ballast, much of the energy was lost to the interaction with fouling materials, reducing the overall effectiveness of the tamping and leading to less stable track conditions.

This study underscores the importance of fine-tuning tamping parameters to suit varying ballast conditions. The team found that by adopting a more data-driven approach – leveraging advanced sensor technology like SmartRock and focusing on energy transfer – railway operators can optimize tamping operations to enhance track stability and longevity. These improvements will not only increase the efficiency of maintenance practices but also contribute to safer, more reliable railway operations.

1. Introduction

The Federal Railroad Administration (FRA) sponsored a team from Pennsylvania State University Altoona to assess the performance of ballast under different tamping conditions, with a particular focus on tamping parameters. In this study, conducted between 2021 and 2023 on Norfolk Southern (NS) railway lines, the team used SmartRock sensors embedded beneath railway ties to capture real-time data on ballast particle movement, acceleration, and stress during tamping operations. These battery-powered wireless sensors were integrated into a sophisticated data acquisition (DAQ) system, providing high-frequency measurements that allow deep insights into the behavior of ballast during various tamping scenarios.

1.1 Background

In rail transportation, the movement of trains over tracks exerts significant forces upon the underlying infrastructure. This infrastructure, which includes rails, ties, and ballast, functions as an elastic system, experiencing deformation and subsequently reverting to its initial state. Over prolonged periods of such stresses, there is a consequential degradation in track geometry that can cause geometrical anomalies, compromising the original geometry of the track. As a result, these compromised zones require provisional speed restrictions to ensure safety. To preempt and mitigate these circumstances, it is important to conduct consistent track maintenance. These measures serve to rejuvenate and reinstate the optimal geometry of the track, ensuring safe operations. (Zhou et al., 2024).

Tamping is a maintenance process that involves lifting, aligning, and leveling the track to correct any deviations from the desired geometry. The process typically starts with the insertion of tamping tools into the ballast, followed by squeezing and vibrating actions that compact the ballast beneath the ties. While tamping is critical for ensuring track stability and reducing the need for frequent maintenance, the process is often guided by empirical practices and heavily relies on the operator's experience. Inappropriate tamping parameters can adversely affect ballast stability, leading to rapid deterioration of track geometry and increased risks, such as track buckling shortly after tamping (Audley & Andrews, 2013; Guo et al., 2021). For this reason, railroads issue slow orders to their trains and use a dynamic track stabilizer directly after tamping. Many tamping parameters are adjustable and are typically selected based on the tamping operator’s experience, prompting railroad maintenance-of-way experts to recommend research to understand how varying tamping parameters impact rail performance and safety.

1.2 Objectives

The primary objective of this research was to investigate the impact of tamping operations on ballast performance at the particle level, and identify optimized tamping parameters that enhance track quality and stability. Specifically, the goal was to understand how varying tamping parameters, such as squeeze time and the number of insertions, affect the mechanical behavior of ballast, including particle motion and stress response during and after tamping. This research was conducted to improve track maintenance operation and ensure safer and more durable railway operations.

1.3 Overall Approach

The team conducted a systematic investigation into the effects of tamping on ballast performance, with a focus on optimizing tamping parameters to improve track quality and stability. Research began with a detailed examination of the tamping process, including the mechanics of tamping machines and the various parameters that influence their effectiveness.

Team members then conducted field tests on selected sections of NS mainline rail, using SmartRock sensors to capture real-time data on ballast particle movement and stress during tamping operations. The tests were designed to evaluate different combinations of tamping parameters, including squeeze time and the number of insertions, under both clean and fouled ballast.

Data collected from these field tests were analyzed to understand the ballast stability during and after tamping, focusing on how different tamping strategies affect the particle motion and stress response of ballast. The insights gained from this analysis were used to develop recommendations for optimizing tamping practices to enhance the durability and safety of railway tracks and guide tamping operations.

1.4 Scope

The scope of this study included field testing and analysis of ballast performance during and after tamping. The research focused on understanding the interaction between tamping parameters and ballast behavior using advanced sensing technology, particularly SmartRock sensors. Researchers studied different ballast conditions, including clean and fouled ballast, to provide a comprehensive understanding of how tamping strategies should be adapted to varying track environments.

1.5 Organization of the Report

The report is organized into three key sections that detail the research methodology and findings. Section 2, "Railroad Tamping," provides an overview of the tamping process, focusing on the key parameters and behaviors of tamping machines that influence ballast compaction and track stability. It discusses the mechanics of tamping, the equipment used, and the importance of various tamping settings such as vibration frequency and squeezing force. Section 3, "Field Tests," outlines the experimental setup for the field tests conducted on NS mainline rail. It includes details on the test site selection, equipment layout, and the specific tamping parameter combinations tested, along with the use of SmartRock sensors to capture real-time data. Finally, Section 4, "Results and Discussion," presents the findings from these field tests, analyzing the data on ballast particle motion and stress variations. This section also explores the effectiveness of different tamping strategies in both clean and fouled ballast conditions, highlighting the relationship between tamping energy and track stability. Section 5 presents a final research summary.

2. Railroad Tamping

Railroad tamping is a critical maintenance practice that involves adjusting and compacting the ballast. This process is essential for ensuring the stability and safety of railway tracks. Over time, the ballast can settle unevenly due to constant vibration from passing trains and environmental factors such as rain and temperature changes. This uneven settling can lead to track irregularities (e.g., dips, bumps, and misalignments) which pose safety risks and can affect train operations.

By regularly tamping ballast, railway operators can correct these irregularities and maintain a smooth, level track alignment, preventing derailments and ensuring the safe passage of trains. It also enhances passenger comfort by reducing vibrations and movements that passengers may experience onboard. Moreover, tamping helps to preserve the longevity of railway infrastructure components such as ties and rails. By distributing the load evenly and reducing stress on track components, proper tamping contributes to the overall durability and lifespan of the railway system.

2.1 Tamping Activity

Figure 1 illustrates the steps involved in a conventional tamping process. This process begins with positioning pairs of tamping tools into the ballast, which are then subjected to compressive and vibratory movements to reposition and consolidate the ballast beneath the tie. In Figure 1 (b), tamping tools are shown penetrating the ballast on both the left and right sides of the tie. At this stage, although the tools are in place, the squeezing action has not yet been initiated. The tools are subjected to a high-frequency vibration, which facilitates easier penetration into the ballast, accompanied by a slight lateral shift that prepares the ballast for compaction.

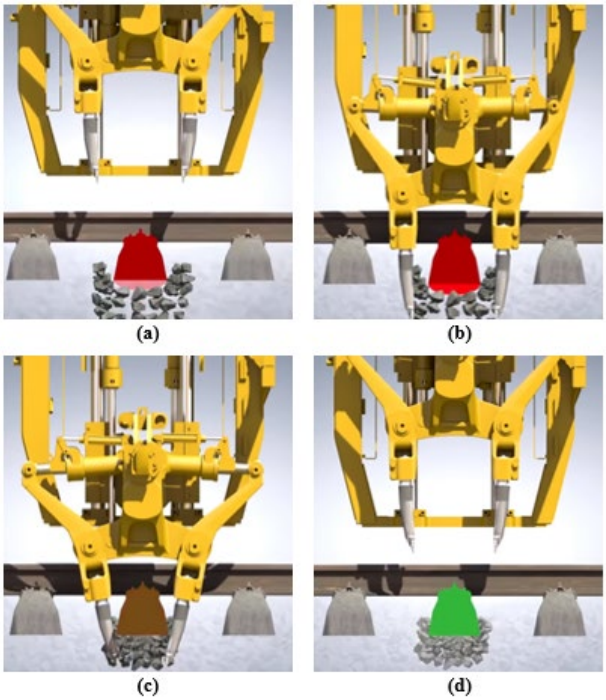

Figure 1. Tamping process subdivision: (a) centering, (b) ballast penetration, (c) squeezing movement, (d) lifting, followed by the relocation of the tamping tools (Plasser & Theurer)

In the stage depicted in Figure 1 (c), the tamping tools fully descend beneath the base of the tie and begin a lateral squeezing action. This squeezing motion is activated by the expansion of the hydraulic cylinders, causing the tamping tools to press the ballast inward, toward the centerline of the tie. The squeezing action consolidates the ballast particles beneath the tie to regain proper track stability. The process occurs at a fixed frequency and amplitude of oscillation, ensuring uniform compaction of the ballast.

Finally, Figure 1 (d) demonstrates the final stage of the tamping process, where the tamping tools are raised and extracted from the ballast. During this stage, the hydraulic cylinders retract and are lifted out, leaving the compacted ballast in place under the tie. This extraction phase completes the cycle, and the tools are ready to move to the next tamping location. The tamping process is then repeated along the track.

2.2 Tamping Machine and Parameters

As railway networks expand and the demand for higher speed and heavier loads increases, the need for precise and reliable tamping operations becomes more pronounced. Optimizing the performance of tamping units directly impacts track geometry correction, ballast compaction, and the long-term durability of railway infrastructure. Advances in this area have the potential to reduce maintenance costs, increase the lifespan of tracks, and improve the safety and reliability of railway operations. Understanding and improving the operation of tamping units is key to enhancing the overall maintenance practices in the railway industry.

The tamping unit serves as the central and most critical component of the tamping machine, responsible for executing the core tamping functions. It comprises several essential elements: tamping tines, which penetrate and compact the ballast; the center of rotation, which provides the necessary pivot for mechanical movements; friction components, which help manage the resistance between moving parts; squeezing cylinders, which generate the force required to compact the ballast; and eccentrics, which create the vibratory motion needed for effective ballast rearrangement.

As economic growth and technological advancements continue to reshape infrastructure development, the railway industry has experienced significant expansion. This rapid construction of railway networks, combined with increasing demands for efficiency and safety, has created new opportunities for the advancement of tamping technology. The need for precise and efficient tamping solutions has become more urgent, especially as rail networks grow and transport heavier loads at higher speeds. To meet these evolving needs, innovations in tamping machinery have emerged, enabling faster, more reliable, and more effective railway maintenance.

Among the leading technologies, three primary tamping systems stand out for their distinctive approaches to achieving optimal ballast compaction: Plasser, Matisa, and Harsco. The Plasser tamping unit operates at a frequency of 35 Hz, using linear movements generated by an eccentric shaft in the vertical plane. This design provides consistent, high-frequency, vertical oscillations that promote effective ballast compaction by ensuring deep penetration and rearrangement of ballast particles. The Matisa tamping unit functions at a frequency of 42 Hz, creating elliptical movements, also driven by an eccentric shaft in the vertical plane. The elliptical motion is designed to enhance ballast penetration while providing a more uniform compaction profile across a wider area, which helps reduce voids and ensures better stability of the track structure. The Harsco tamping unit, however, adopts a different approach, operating at a higher frequency

of 53 Hz. This system employs torsional movements in the horizontal plane, generating rotational forces that promote efficient lateral compression of the ballast. This torsional movement helps align ballast particles horizontally, which is particularly beneficial for enhancing lateral stability, especially on curves and tracks with significant lateral forces.

These three systems reflect the diverse strategies being implemented to meet the unique challenges of track maintenance across various railway environments. Figure 2 shows the Plasser GRM3000T tamping machine, which is currently deployed in the field.

Figure 2. Plasser GRM3000T tamping machine

Despite significant advancements in the design and functionality of tamping machines, optimizing their effectiveness in real-world applications continues to present notable challenges. While the core mechanisms of tamping machines have matured, the complexities of actual field conditions (e.g., varying ballast material properties, track geometry, and operational environments) make it difficult to achieve uniform compaction results. One of the main obstacles to maximizing tamping effectiveness are the tamping parameters themselves, which have remained largely unchanged and inconsistently applied for nearly seven decades.

The tamping parameters widely adopted by rail operators around the world often lack a solid scientific foundation tailored to specific ballast characteristics or the unique conditions of different railway lines. Ballast materials can vary widely in terms of size, angularity, and older, composition, and track conditions differ significantly between newly constructed lines and heavily trafficked tracks. As a result, the one-size-fits-all approach to tamping can lead to inconsistent performance in maintaining track stability and could prolong track geometry corrections. This has resulted in increased maintenance needs and the potential for premature track degradation in certain cases.

For example, vibration frequency, a key parameter in tamping, is essential for breaking into the ballast and compacting it. However, the appropriate frequency can differ based on ballast size and angularity, which are not always considered in current tamping practices. Similarly, the squeezing force applied to ballast particles during tamping is another varying factor. Too much force can damage the ballast, while too little may result in inadequate compaction. Additionally,

parameters such as squeezing time, lifting height, and penetration depth further complicate the tamping process, as they all interact with the track and ballast in different ways depending on the specific track conditions.

Table 1 outlines the major tamping parameters that must be considered during tamping operations.

Table 1. Tamping parameters

Parameter	Description
Vibration frequency	Oscillating frequency when inserting ballast or closing the tamping tines, which is used to break into ballast or compact the ballast bed.
Vibration amplitude	The amplitude when closing the tamping tines, which is used to compact the ballast bed.
Squeezing force	The maximum lateral force (in the horizontal direction) applied to ballast particles during squeezing.
Squeezing velocity	The speed of the tamping tine squeezing the ballast bed.
Squeezing time	The overall time of squeezing.
Lifting height	The track-lifted height before penetrating the tamping tine
Penetration depth	The tamping tine depth when penetrating the ballast bed
Insertion number	The number of squeezing the ballast particles by tamping tines for one target tie.

The variations in these parameters, and the ways in which they are applied, have a direct impact on the long-term performance of the track. Without careful calibration of each parameter according to the specific conditions of the track and ballast material, the tamping process may result in suboptimal compaction, leaving the track more vulnerable to future degradation. Therefore, it is important to refine tamping practices to better account for the diverse conditions encountered in the field, using modern, data-driven approaches and advanced sensing technologies to optimize each parameter for the specific requirements of the track being maintained.

2.3 Tamping Tool Behavior

The performance of ballast is intricately linked to the mechanical movements of the tamping machine, specifically the operation frequency and the detailed motion curve of the tamping tool. Understanding the behavior of the tamper, including the precise motion it follows during the tamping process, is essential for optimizing ballast performance and ensuring long-term track integrity.

Figure 3 provides a clear depiction of the idealized squeezing motion of the tamping tool throughout the tamping process. The horizontal axis represents time in seconds, while the vertical axis shows the vertical displacement of the tamping tool in millimeters. The solid curve

illustrates the oscillatory motion of the tamping tool as it moves through various phases of the tamping cycle. This sinusoidal-like motion shows the repetitive upward and downward movement as the tool engages and disengages with the ballast.

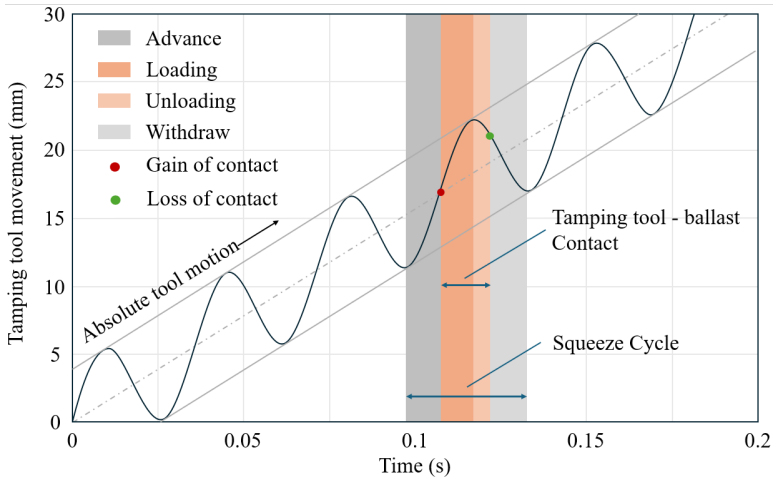

Figure 3. Ideal tamping tool motion during squeezing process

Several phases are identified in the figure, each representing a distinct part of the tamping cycle. The shaded regions indicate specific phases of the tool's movement:

- The dark gray region represents the "Advance" phase, where the tamping tool moves downward toward the ballast bed, preparing for contact.
- The dark orange region indicates the "Loading" phase, during which the tool is in direct contact with the ballast, applying pressure to compact the particles. This is where the maximum squeezing force is applied to the ballast.
- The light orange region corresponds to the "Unloading" phase, where the pressure is gradually reduced as the tool begins to lift away from the ballast.
- The light gray region marks the "Withdraw" phase, where the tamping tool fully retracts from the ballast bed, completing the cycle.

The points marked on the curve show the gain of contact (red point) and loss of contact (green point) between the tamping tool and the ballast. These points show how the tamping tool interacts with the ballast during each oscillatory motion. The absolute motion of the tool, depicted by the solid curve, highlights the oscillatory nature of the squeezing action, while the dashed lines indicate the general trajectory and trend of the tool's movement over time.

This ideal motion pattern shows that each squeeze cycle involves a combination of loading and unloading phases that, when optimized, ensure the ballast is properly compacted. The timing, amplitude, and frequency of the oscillations are all important factors that influence how effectively the ballast is packed and how stable the track becomes post-tamping. By studying and optimizing these mechanical dynamics, railway maintenance engineers can achieve better ballast compaction, leading to enhanced track stability and a reduction in maintenance needs over time. Understanding the interactions between the tamping tool and ballast is fundamental to improving the tamping process and achieving more consistent and reliable track performance.

The tamping process includes both penetration (i.e., insertion) and squeezing movements. The excitation frequency used in this research was 35Hz, or 35 squeeze cycles per second. With dynamic excitation, the lowering of the tamping unit allows the tamping tools to effectively penetrate the ballast and reach the necessary position beneath the tie. This dynamic excitation facilitates the squeezing movement, overcoming the passive earth pressure and rearranging the ballast grains to fill the voids under the tie.

Figure 4 illustrates the relationship between tine displacement and cylinder pressure during the tamping tool's squeezing process, providing a detailed view of how the tamping machine interacts with the ballast over time. In the top graph, the tine displacement begins with a rapid upward movement, representing the initial phase where the tines penetrate the ballast. After this rapid increase, the tines enter a slower increase phase, during which they gradually reach their maximum displacement. This indicates that the squeezing action continues, but the rate of displacement decelerates as the ballast particles become more densely packed. Once the squeezing phase is complete, the tines begin to retract (i.e., withdraw), returning to their initial position, which ends the tamping cycle.

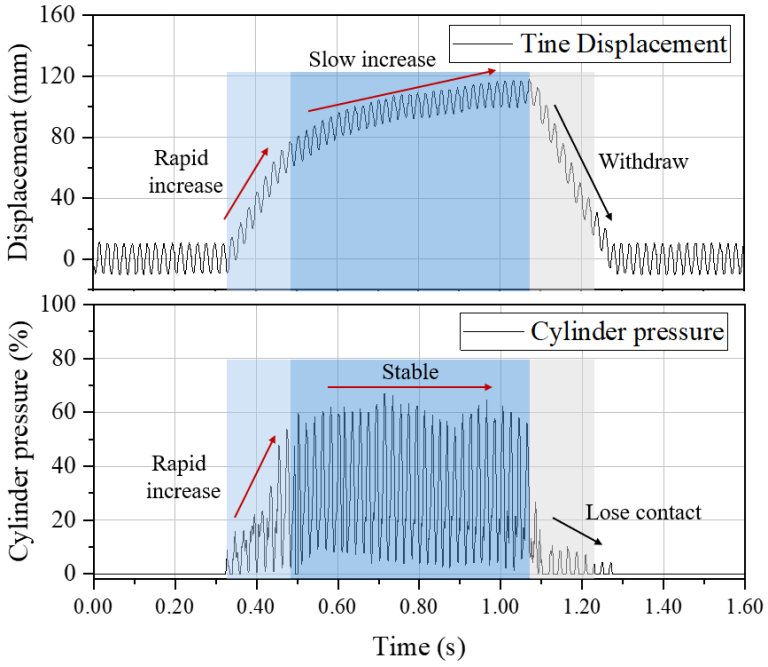

Figure 4. Tamping tine motion and cylinder pressure in squeezing process

In the bottom graph of Figure 4, the cylinder pressure closely mirrors the tine displacement behavior. The pressure within the cylinder initially rises rapidly, reflecting the force applied by the tines as they push into the ballast. This rapid increase corresponds to the void-filling stage, where the ballast is forced into gaps beneath the ties. After this, the cylinder pressure stabilizes, maintaining a steady level during the slow increase in tine displacement. This stable pressure indicates that the tamping tool is now compacting the ballast, ensuring that it is densely packed. As the tines begin to withdraw, the cylinder pressure drops sharply, indicating a loss of contact between the tamping tool and the ballast.

The behavior illustrated in Figure 4 suggests that the interaction between the tamping tool and the ballast can be divided into two distinct stages. The first is the void-filling stage, characterized

by the rapid increase in both tine displacement and cylinder pressure. During this phase, the tamping tines fill the gaps created by track leveling, redistributing the ballast beneath the ties. This stage is relatively quick, taking less than 0.2 seconds on average.

The second stage is ballast compacting, which occurs after the voids have been filled. During this phase, the ballast particles are compacted under the steady pressure of the tines, ensuring that the ballast is tightly packed and stable. The effectiveness of the tamping process largely depends on this compacting phase, as it determines the overall density and stability of the ballast after tamping. Therefore, variations in squeezing time that primarily occur in this second stage may result in varying compaction and track stability.

This dual-phase interaction – void filling followed by ballast compacting – highlights the importance of optimizing both tine movement and cylinder pressure during the tamping process. By carefully controlling these parameters, railway maintenance teams can achieve more consistent and reliable results, ensuring that the track remains stable and secure over time.

3. Field tests

3.1 SmartRock Sensors

The team used SmartRock, a proprietary wireless sensing technology, to better capture the behavior and performance of ballast at the particle level during tamping operations. These battery-powered sensors are designed to provide real-time, high-precision measurements of ballast particle movement and interaction under the forces exerted by the tamping machine. Each SmartRock sensor is equipped with a triaxial gyroscope, accelerometer, magnetometer, and stress cells, enabling it to directly measure key parameters such as translational acceleration, angular rotation, and particle contact stress. These sensors provide a detailed picture of the mechanical response of ballast particles, which is critical for understanding how tamping affects ballast compaction and track stability.

Although variations of the SmartRock sensor exist that mimic the shape of natural rocks to provide realistic data, the version chosen for this field test has a standard cubical shape with a 35 mm side length. The cubical design minimizes the influence of particle shape on measurements (Tutumluer et al., 2006) and allows for more consistent data collection. The 3D-printed shell of the sensor made with PLA is robust enough to withstand the forces applied during tamping and can be replaced easily after several uses, while the cubical form also simplifies the measurement of triaxial movements and stresses. Additionally, the cubical shape facilitates the transformation of data from the local coordinate system to a global coordinate system, which is important for analyzing the movements and stresses in a standardized framework. This standardization enhances the accuracy and reliability of the collected data.

One feature of the SmartRock technology is its ability to transmit data wirelessly through Bluetooth Low Energy (BLE) communication. The transmission distance varies from several inches to a couple of feet depending on ballast condition. The sensor can communicate in real time with a remote-controlled data acquisition (DAQ) system, allowing engineers to monitor the tamping process as it occurs. This capability not only provides immediate insights but also ensures that any issues or anomalies in the tamping process can be identified and addressed without delay. Figure 5 illustrates the cubical form of the SmartRock sensor, highlighting its practical design for field testing.

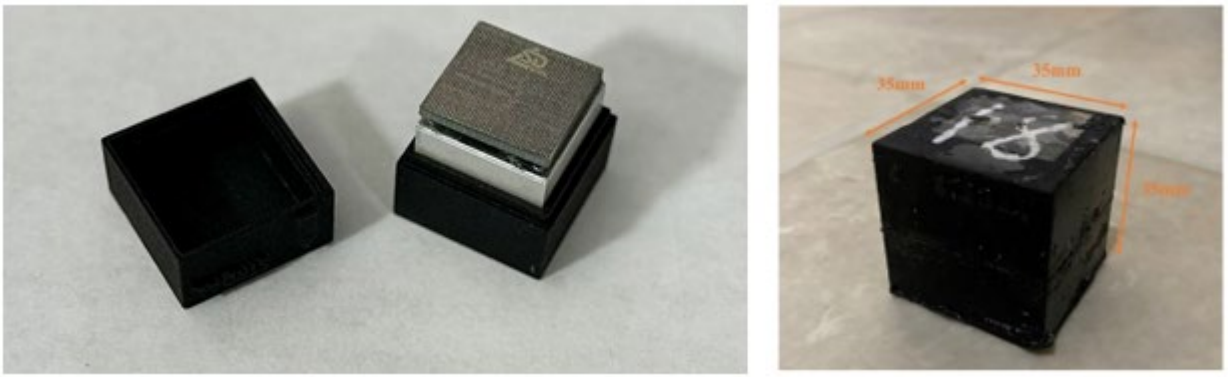

Figure 5. Battery-powered, wireless SmartRock sensor

The development of the SmartRock sensor is well-documented in previous research (Huang et al., 2018; Liu et al., 2015, 2016, 2018; Liu, Gao, et al., 2017; Liu, Huang, et al., 2019; Liu,

Huang, & Qiu, 2017; Liu, Huang, Qiu, & Gao, 2017; Liu, Huang, Qiu, & Kwon, 2017; Liu, Qiu, et al., 2019; Zeng et al., 2019, 2020, 2024; Zhou et al., 2024). The sensor's sampling frequency can be adjusted up to 200 Hz depending on the measurement requirements. For this field test, the acceleration and stress sensors operated at 100 Hz, which is sufficient to meet the Nyquist frequency criteria and ensure accurate data collection without aliasing. A sampling frequency of 16.6 Hz was used for the rotation measurements, which provided a comprehensive view of particle rotation throughout the tamping process. This setup enabled researchers to capture the detailed mechanics of ballast compaction and the effects of the tamping forces, providing new insights into optimizing tamping strategies for better track stability and longevity.

3.2 Test Site Identification

The field tamping tests were conducted on an NS Class IV revenue service mainline track at three locations. The first test was carried out at Bellwood, PA, on October 30, 2021 (Figure 6 (a)), the second test took place at Tunnelhill, PA, on April 7, 2022 (Figure 6 (b)), and the final test was conducted at Chesapeake, VA, on December 5, 2023 (Figure 6 (c)). These locations are part of the NS mainline, which serves both freight and passenger trains. Freight trains on this line typically have an axle load of 32,000 kg and travel at speeds of approximately 40 km/h, while passenger trains have an axle load of 16,150 kg and travel at speeds of approximately 115 km/h.

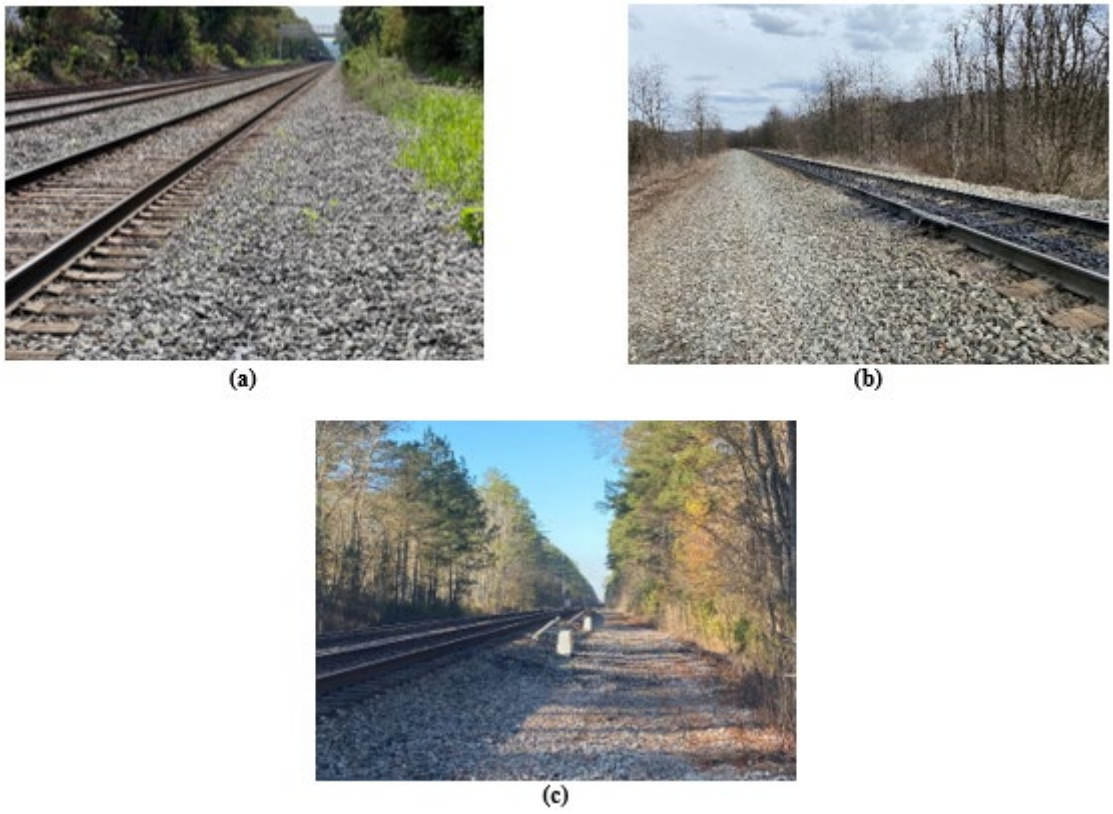

Figure 6. NS Class IV revenue service mainline track: (a) Bellwood, PA; (b) Tunnelhill, PA; (c) Chesapeake, VA

The double main route in Figure 6 (a) handles a total traffic density of about 117 gross million tonnes (GMT) annually in both directions. The specific section of the track used for testing,

Main #2, carries over 58 GMT per year. This track is built using wood ties that measure 259 cm long, 23 cm wide, and 18 cm high, along with Continuously Welded Rail (CWR) for enhanced stability. The Chesapeake line carries approximately 59 MGT annually in both directions. At the test location in Figure 6 (b), Main #2 (eastbound, south track), where sensors were installed, carries 41.1 MGT. The Tunnelhill section in Figure 6 (c) includes two tracks with a combined annual tonnage of 120 MGT, averaging about 60 MGT per track.

The ballast in Bellwood and Chesapeake sections are clean AREMA #25 ballast, with a void ratio of around 39 percent, which is essential for providing adequate drainage and support for the heavy loads that pass over the track, while ballast in Tunnelhill is fouled. The ballast in these sections are set to be lifted to 2.5 cm during tamping to allow for proper redistribution and compaction. These tests were designed to evaluate the performance of different tamping parameters under the given track conditions, providing key data for improving maintenance strategies and ensuring long-term track stability.

3.3 Equipment Layout

Figure 7 illustrates the layout of the data acquisition system used to monitor ballast performance during the tamping process. The monitoring system integrates wireless SmartRock sensors, DAQ boxes, solar panels, antennas, and a remote controller to enable continuous and automated data collection. The system was designed to be energy-efficient, using solar power to provide several days of operation without interruption during and after tamping.

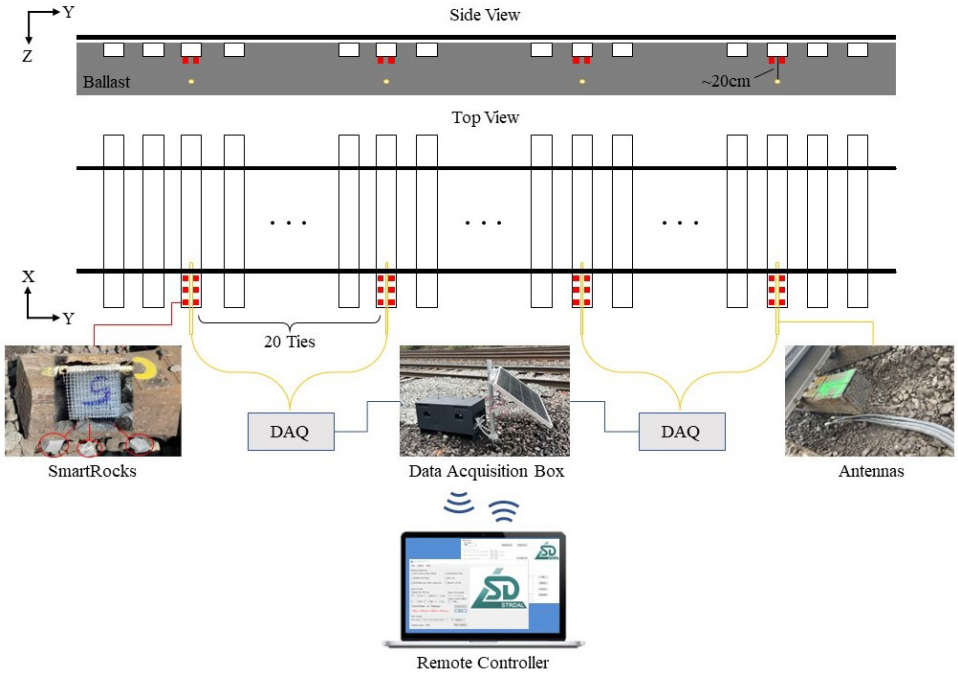

Figure 7. Field layout of data acquisition system

The test setup involved four selected sections of the track, each spaced 20 crossties apart to ensure consistent ballast conditions. In each test section, six SmartRock sensors were buried directly beneath each crosstie, providing detailed particle-level monitoring. These sensors were carefully protected from the elements by being wrapped in four layers of waterproof and glass

fiber tape, as depicted in the leftmost photograph of Figure 7. The sensors were designed to measure key parameters such as translational acceleration, angular rotation, and particle stress, which are important for assessing the effectiveness of tamping.

The DAQ systems, positioned trackside, served as the main communication hub between the SmartRock sensors and the remote monitoring station. These systems wirelessly communicated with the sensors, allowing real-time data collection and transmission. The connection was maintained through Wi-Fi hotspots, and data were transmitted to a remote lab for further analysis via a remote controller (typically a laptop). Cellular service was tested before installation and the data are stored in the local computer for backup. To ensure uninterrupted power supply, solar panels were installed to recharge the storage batteries powering the DAQ systems, preventing power loss and maintaining continuous operation.

Antennas buried 20 cm below the ties played a critical role in maintaining a strong wireless connection between the SmartRock sensors and the DAQ boxes, especially during adverse weather conditions or other disturbances that could interfere with communication. The rightmost photograph in Figure 7 shows an example of the antenna setup, which ensured reliable data transmission even in challenging environments.

The entire system was designed to operate only during the railroad working period, optimizing energy efficiency. When not actively collecting data, the SmartRock sensors were placed into sleep mode, with periodic activations to capture data during the post-tamping period. This approach allowed for extended monitoring while minimizing power consumption, making it an efficient and effective solution for long-term track maintenance analysis.

3.4 Parameter Combinations

The team used the Plasser GRM3000T to execute different tamping parameter combinations. The GRM300T is a multi-functional tamping machine with fully automatic track lifting, lining, and cross-leveling capabilities. It is especially designed for the stringent requirements of high density, high tonnage railroads, short lines, and contractors. All tamping tools apply the same pressure, and they vibrate with an ideal frequency of exactly 35 Hz. During the tamping process, the tamping tool can be adjusted to execute different tamping parameters (e.g., squeeze time, number of squeezes, etc.).

The test matrix for evaluating the effects of tamping parameters on ballast performance was structured to include two sites: Bellwood (clean ballast) and Tunnelhill (fouled ballast). Each site included four test scenarios, as shown in Table 2.

For the clean ballast site at Bellwood, four different test scenarios were employed. The squeeze time varied between 0.6 and 1.0 seconds, while the number of insertions was either one or two. Specifically, Scenario #1 used a squeeze time of 0.6 seconds with one insertion, Scenario #2 also used a squeeze time of 0.6 seconds but with two insertions. Scenario #3 had a squeeze time of 1.0 seconds with one insertion, and Scenario #4 used a squeeze time of 1.0 seconds with two insertions.

At the fouled ballast site in Tunnelhill, another four test scenarios were executed. The squeeze time ranged from 0.6 to 1.2 seconds, with either one or two insertions. Scenario #5 employed a squeeze time of 0.6 seconds with one insertion, Scenario #6 extended the squeeze time to 0.8 seconds with one insertion, Scenario #7 used a squeeze time of 0.8 seconds with two insertions, and Scenario #8 used a squeeze time of 1.2 seconds with one insertion.

At the clean ballast site in Chesapeake, the team ran another four test scenarios using the same settings used in the Tunnelhill site. This made it easy to compare tamping results from the clean ballast site at Chesapeake to the fouled ballast site in Tunnelhill.

Across all scenarios, the lifting value was consistently set at 25 mm, and the pressure was maintained at a constant frequency of 35 Hz. This combination of parameters allowed for a detailed investigation of how different tamping conditions affect ballast compaction and stability, providing insights into optimizing tamping practices for varying track conditions.

Table 2. Tamping parameter settings

Site	Scenario No.	Insertions (no.)	Squeeze time (s)	Lifting Value (mm)	Pressure/frequency
Bellwood, PA (clean ballast)	#1	0.6	1	25	Const./ 35Hz
	#2	0.6	2		
	#3	1.0	1		
	#4	1.0	2		
Tunnelhill, PA (fouled ballast)	#5	0.6	1		
	#6	0.8	1		
	#7	0.8	2		
	#8	1.2	1		
Chesapeake, VA (clean ballast)	#9	0.6	1		
	#10	0.8	1		
	#11	0.8	2		
	#12	1.2	1		

4. Results and Discussion

4.1 Ballast Particle Motion During Tamping

The SmartRock sensors recorded acceleration data over a specific period during the tamping process at various test sections. Figure 8 illustrates the acceleration variations measured by the SmartRock sensors under tamping parameter Scenario #2, which involves two insertions and a 0.6-second squeeze time. To differentiate the location of the sensor-equipped ties, the tie where the SmartRock sensors were placed is labeled as Tie #0, while adjacent ties are labeled as #-1, #1, and so on, as shown in the right-bottom section of Figure 8.

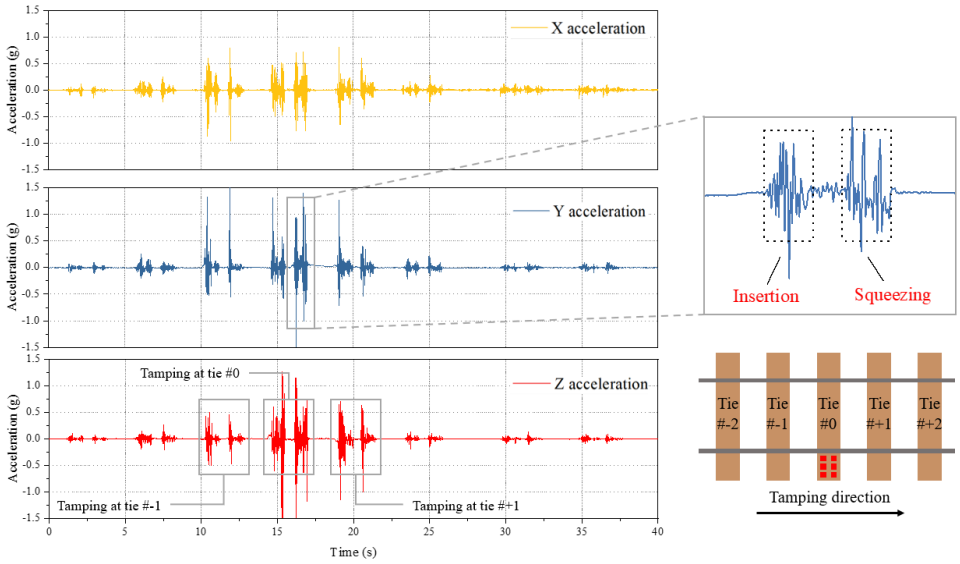

Figure 8. Acceleration signal during tamping

The acceleration data reveal that higher acceleration responses were observed at Ties #-1, #0, and #1, compared to the surrounding ties. This indicates that tamping primarily affects ballast movement within the range of three adjacent ties, demonstrating the localized impact of tamping. The data also clearly show distinct acceleration patterns corresponding to the tamping machine's insertion and squeezing actions, which can be identified in the magnified view on the left of Figure 8.

Moreover, the acceleration responses in both the x and y directions are noticeably larger than those in the z direction. This can be attributed to the dominance of horizontal movements during the tamping tool's squeezing phase, which primarily influences lateral ballast displacement. The vertical movement (z direction) plays a lesser role, as indicated by the relatively lower accelerations in that axis.

The accelerations presented in Figure 8 were originally measured in the local coordinate system of the SmartRock sensors, which required transformation into the global coordinate system for accurate analysis. To achieve this, quaternion mathematics was employed, a method that is well-suited for representing the rotation and orientation of objects. A unit quaternion was specifically used in this case to translate the sensor data from the local coordinate system to the global coordinate system, as detailed in prior research (Zeng et al., 2019). This transformation allowed

for a more accurate understanding of the sensor data in the context of the track environment, ensuring that the measurements were consistent and comparable across all test sections.

Analysis of the acceleration data from the SmartRock sensor on clean and fouled ballast provides intriguing insights into the understanding of tamping operations under varying conditions. Figure 9 illustrates the typical pattern of ballast particle acceleration during tamping, specifically in the case of two insertions followed by a 1-second squeezing time. The x-axis represents time in seconds, while the y-axis represents acceleration in gravitational force (g), ranging from -8g to 8g. The blue line on the graph shows the recorded acceleration data throughout the process. Two distinct phases are highlighted by red dashed rectangles: insertion and squeezing. The insertion phase is characterized by the action of the tamper tine lowering into the ballast, causing small oscillations in acceleration. In contrast, the squeezing phase involves the tines squeezing to rearrange the ballast toward the center beneath the tie, resulting in more significant fluctuations.

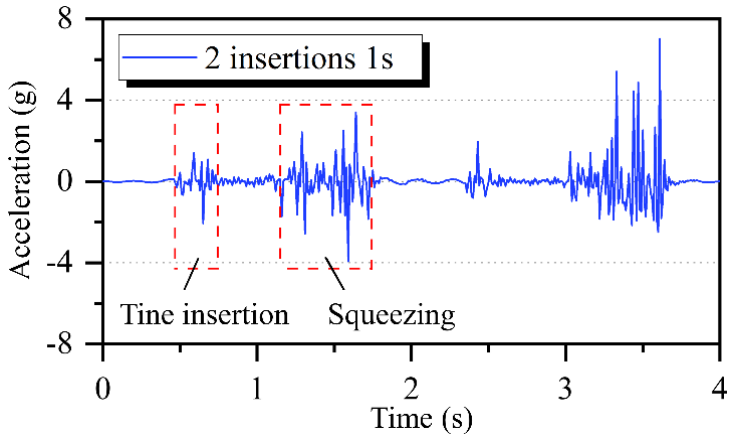

Figure 9. Acceleration pattern of ballast particle with two insertions

Figure 10 presents acceleration data captured from both clean and fouled ballast in Bellwood and Tunnelhill, PA, under different tamping conditions. In clean ballast (Bellwood), the acceleration responses were generally smaller and less frequent, particularly in the case of a 0.6-second squeezing time with one insertion, which suggests minimal disturbance and effective interaction between the tamping machine and the ballast. However, as the squeezing time increased to 1 second or the number of insertions increased to two, the recorded acceleration during the squeezing phase intensified, indicating that the ballast experienced more significant compaction forces. This shows that longer squeezing times and multiple insertions promote more intense ballast rearrangement and compaction in clean ballast.

On the other hand, the fouled ballast (Tunnelhill) exhibited consistently higher and more frequent acceleration peaks, regardless of the tamping conditions. The presence of fouling materials such as dirt, debris, or other contaminants increased the complexity of the ballast structure, leading to more pronounced fluctuations in the acceleration data. These larger peaks were observed across all scenarios, suggesting that fouled ballast is more resistant to tamping forces, causing greater particle movement and disturbance.

Moreover, the increased insertion time and number of insertions in the fouled ballast scenarios amplified the acceleration responses even further. The fouling material disrupted the efficient transfer of tamping forces, requiring more energy and resulting in heightened particle motion during both the insertion and squeezing phases. This highlights the challenge of tamping in

fouled ballast conditions, where achieving proper compaction is more difficult and requires greater tamping effort, leading to higher acceleration peaks and more significant fluctuations in the recorded data.

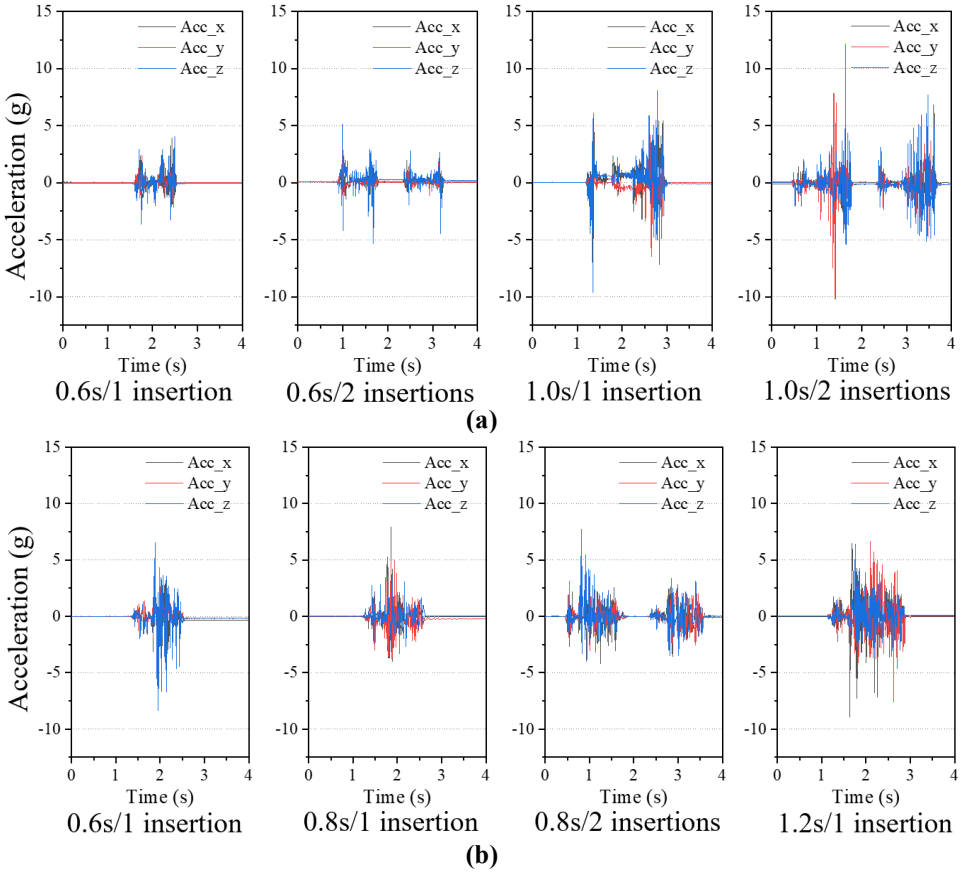

Figure 10. Ballast particle acceleration pattern in varying cases: (a) Bellwood (clean ballast); (b) Tunnelhill (fouled ballast)

Figure 11 presents box plots illustrating the average horizontal accelerations during the squeezing phase of tamping, derived from SmartRock sensors across various ballast conditions. The analysis focuses on clean ballast (Bellwood and Chesapeake) and fouled ballast (Tunnelhill), comparing the effects of different tamping insertions and squeeze times. In terms of two insertions cases, the average horizontal accelerations of the first and second squeezing are illustrated separately in the form of shade boxes. Therefore, there are six box plots for clean ballast in Bellwood and five box plots for clean ballast in Chesapeake and fouled ballast in Tunnelhill.

In the case of clean ballast (Figure 11 (a) and Figure 10 (c)), the data shows that two tamping insertions generally produced higher average horizontal accelerations compared to a single insertion, particularly noticeable at the 1.0-second squeeze time. This indicates that repeated tamping not only leads to higher compaction but also yields more consistent results, as evidenced by the narrower interquartile ranges (IQRs). These findings suggest that for clean ballast, increasing the number of tamping cycles may enhance track stability by achieving better compaction of the ballast particles.

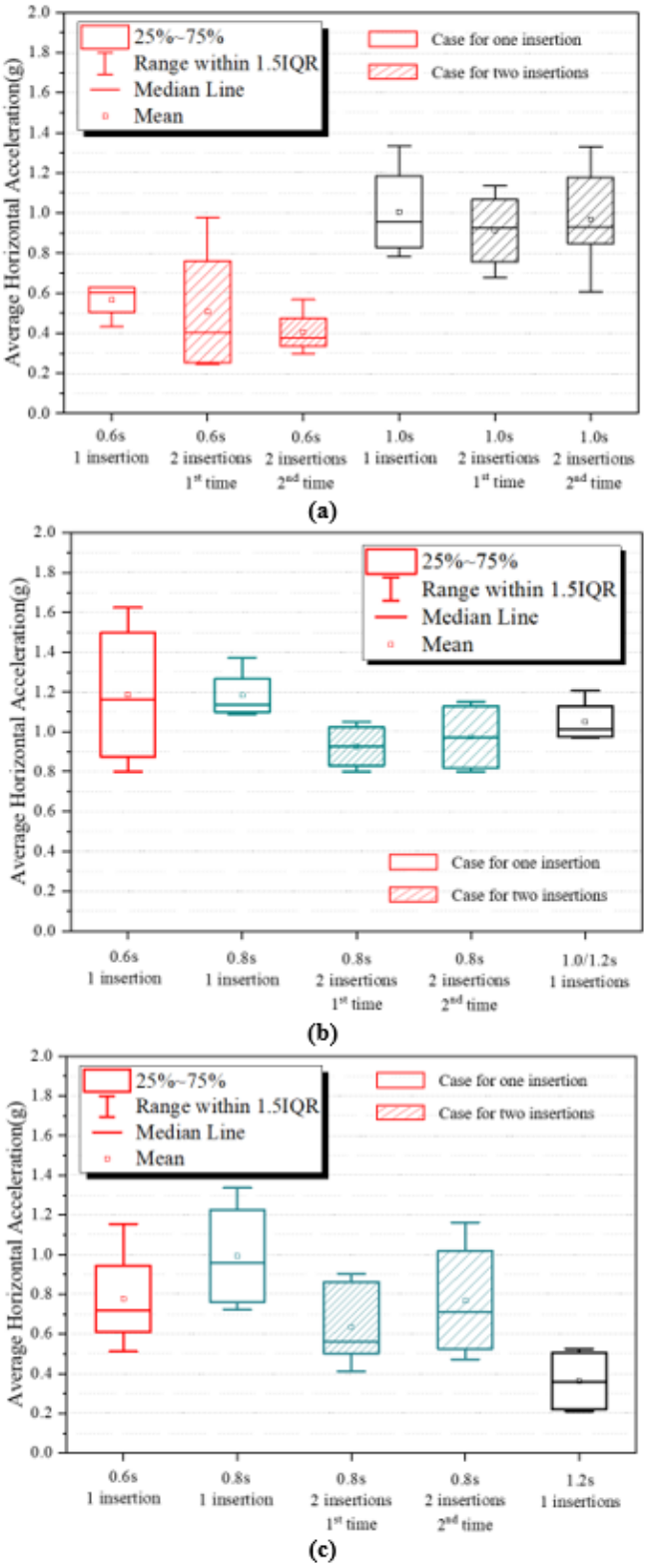

Figure 11. Comparison of squeezing acceleration: (a) Bellwood (clean ballast); (b) Tunnelhill (fouled ballast); (c) Chesapeake (clean ballast)

On the other hand, fouled ballast (Figure 11 (b)) exhibited generally higher acceleration values across all tamping conditions when compared to clean ballast. Moreover, the variability in acceleration readings was significantly lower in fouled ballast, as indicated by the smaller IQRs. This reduction in variability implies that the presence of fouling materials dampens the mechanical response of the ballast to tamping. The fouling material may inhibit the effective transmission of tamping forces through the ballast, resulting in less efficient compaction. Consequently, these observations highlight the need for modified tamping strategies or additional maintenance practices to mitigate the adverse effects of fouling on ballast performance.

The rotation patterns of ballast particles, depicted in orange in Figure 12, show distinct differences between clean ballast (Bellwood) and fouled ballast (Tunnelhill) under the same tamping conditions of one insertion with a 0.6-second squeezing time.

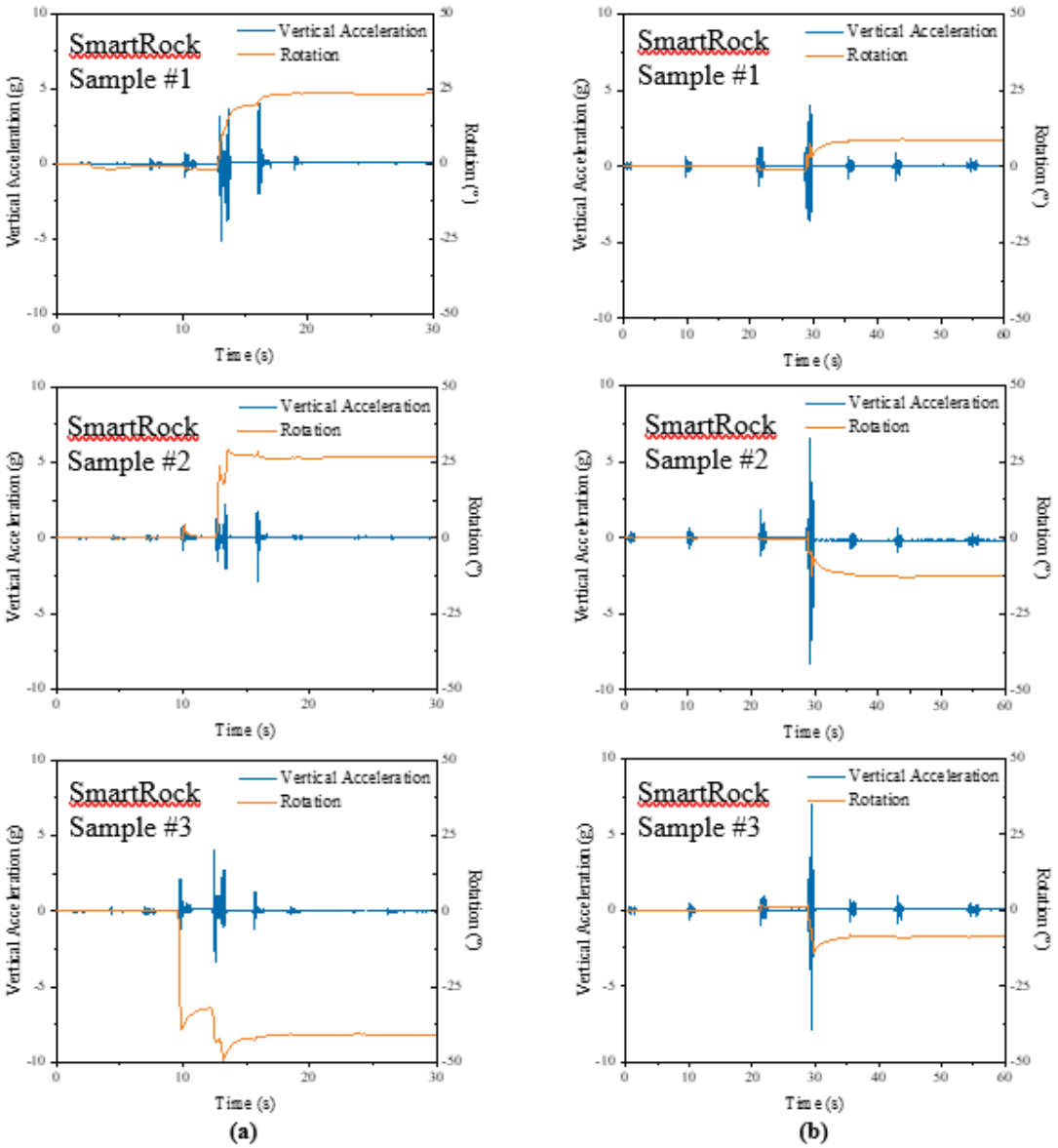

Figure 12. Ballast particle rotation pattern for one insertion and 0.6 second squeezing time: (a) Bellwood (clean ballast); (b) Tunnelhill (fouled ballast)

In the clean ballast scenario (Bellwood), the rotation pattern is more irregular and less predictable. After the initial tamping impact, there are sharp increases in rotation. This sharp change in rotation indicates that the particles were effectively reorienting and adjusting under the tamping forces, contributing to better compaction. The rotation pattern suggests that clean ballast particles are more responsive to tamping, likely due to the absence of obstructive materials that could hinder movement.

Conversely, in the fouled ballast condition (Tunnelhill), the rotation of ballast particles demonstrates a relatively smooth and steady increase following the initial impact of tamping. The rotation fluctuates lightly, indicating that the particles were not reorienting as consistently or effectively as in the clean ballast scenario. It suggests that the presence of fouling materials was interfering with the particles' ability to rotate and settle properly, which may reduce the overall effectiveness of the tamping process.

The scatter plots in Figure 13 provide a comprehensive view of the relationship between particle rotation and average horizontal acceleration under different tamping conditions, across both clean and fouled ballast.

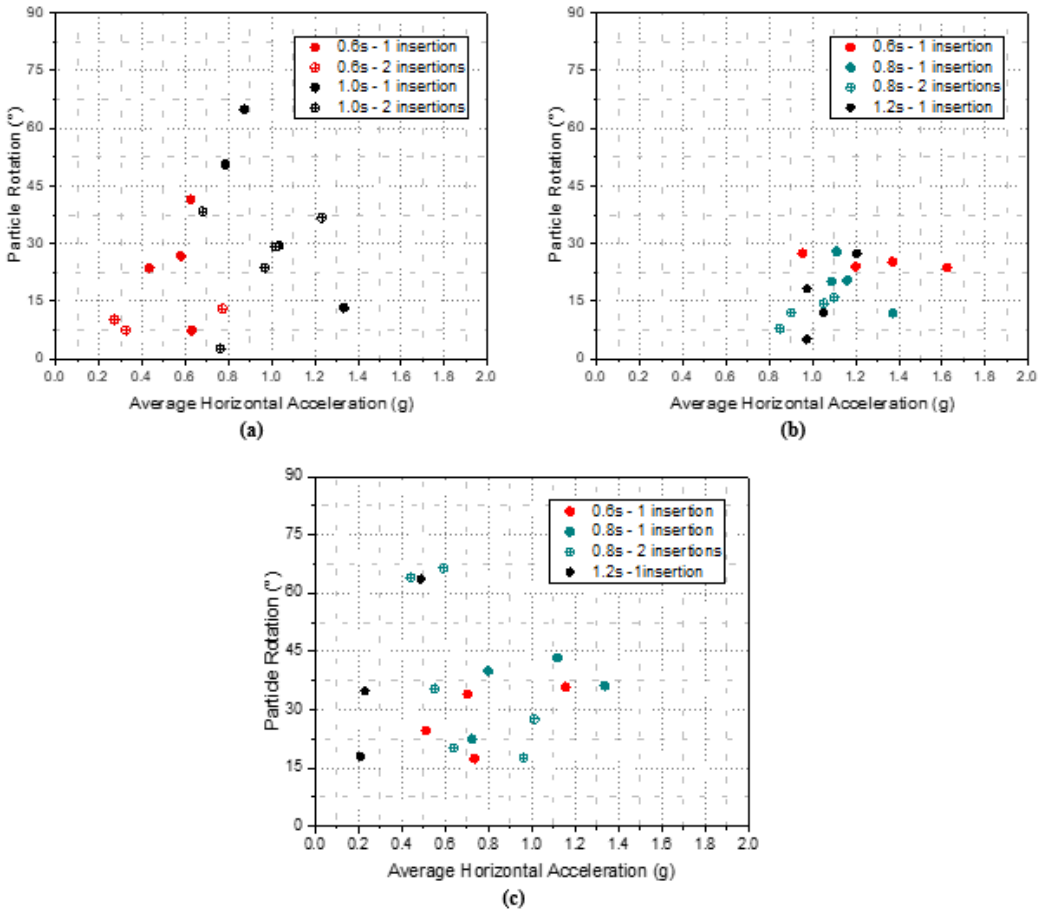

Figure 13. Comparison of particle rotation: (a) Bellwood (clean ballast); (b) Tunnelhill (fouled ballast); (c) Chesapeake (clean ballast)

Three particles for clean and fouled ballast cases were selected for analysis. In clean ballast (Figure 13 (a)), there is a clear correlation where higher accelerations are generally associated

with greater particle rotation. This trend is especially pronounced with longer squeeze times and multiple insertions, indicating that more intense tamping promotes greater reorientation and movement of ballast particles. Such behavior suggests that intensified tamping may improve the packing density and interlocking of ballast particles, potentially enhancing track stability. However, the observed variability in particle rotation at lower acceleration levels indicates that there might be a threshold below which tamping is less effective, underscoring the importance of precise control over tamping parameters to ensure optimal compaction.

In contrast, the fouled ballast (Figure 13 (b)) exhibited less variation in particle rotation across different tamping conditions, with a generally lower range of rotation angles compared to clean ballast. This suggests that fouling materials may impede the movement and reorientation of ballast particles, likely due to the binding or bridging effects introduced by the fouling. Although higher accelerations still correspond to increased particle rotation, the overall lower rotation in fouled ballast points to reduced tamping efficacy. This diminished rotation indicates that fouled ballast may not achieve the same level of optimal packing and stability as clean ballast, raising concerns about the long-term durability and maintenance needs of tracks subjected to fouling.

These findings highlight the critical role of ballast condition in tamping operations. For clean ballast, achieving higher accelerations through appropriate tamping intensity and frequency can lead to better compaction and stability. However, for fouled ballast, even similar tamping efforts may not yield comparable results, suggesting a need for alternative or additional maintenance strategies to mitigate the negative impacts of fouling on ballast performance.

4.2 Stress Variation During and After Tamping

Figure 14 presents a comparison of vertical acceleration and bulk stress over time for both clean and fouled ballast. The time-series data illustrate the dynamic responses of the ballast during a tamping event, providing insights into the mechanical behavior under operational conditions.

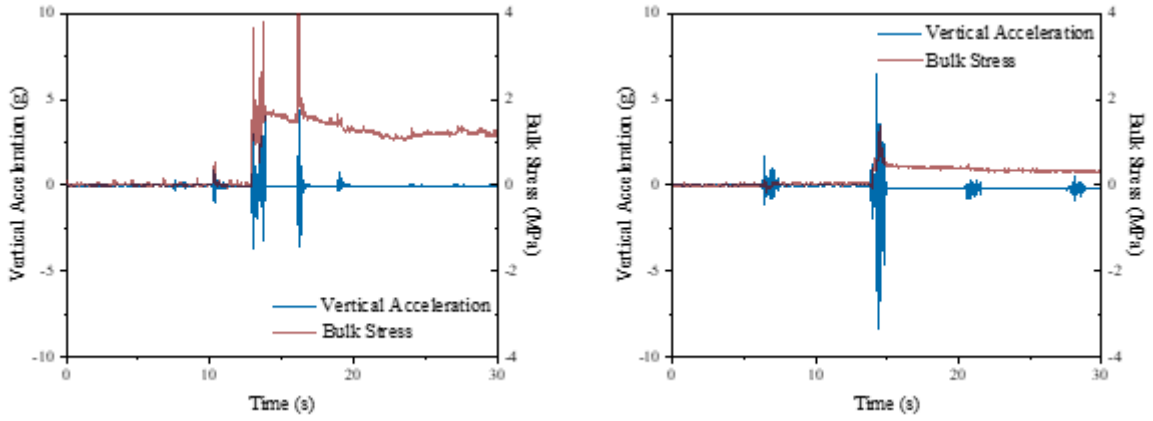

Figure 14. Comparison of particle bulk stress between clean (left) and fouled (right) ballast

In the clean ballast (left graph), the vertical acceleration shows significant spikes that coincide with high levels of bulk stress. This indicates that when clean ballast is subjected to tamping, it experiences high dynamic forces and a corresponding increase in stress levels. The peak in vertical acceleration suggests a robust interaction between the tamping equipment and the ballast, leading to substantial particle movement and effective stress transmission throughout the

ballast layer. The clean ballast demonstrated a capacity to absorb and transmit these forces, likely contributing to effective compaction and stabilization of the track foundation.

Conversely, the fouled ballast (right graph) exhibited a different behavior pattern. While there are similar spikes in vertical acceleration, the corresponding stress levels are generally lower and less pronounced compared to the clean ballast. This pattern suggests that fouling materials within the ballast may dampen the transmission of forces and reduce the effectiveness of stress distribution. Such a scenario can lead to inadequate compaction and less effective stabilization of the ballast. The fouled condition appears to buffer and absorb the energy imparted by tamping, potentially leading to a less stable track structure that might require more frequent maintenance.

Figure 15 illustrates the evolution of normalized bulk stress over time for both clean and fouled ballast under different tamping conditions, providing insights into the longer-term mechanical behavior and stability of the ballast after tamping operations.

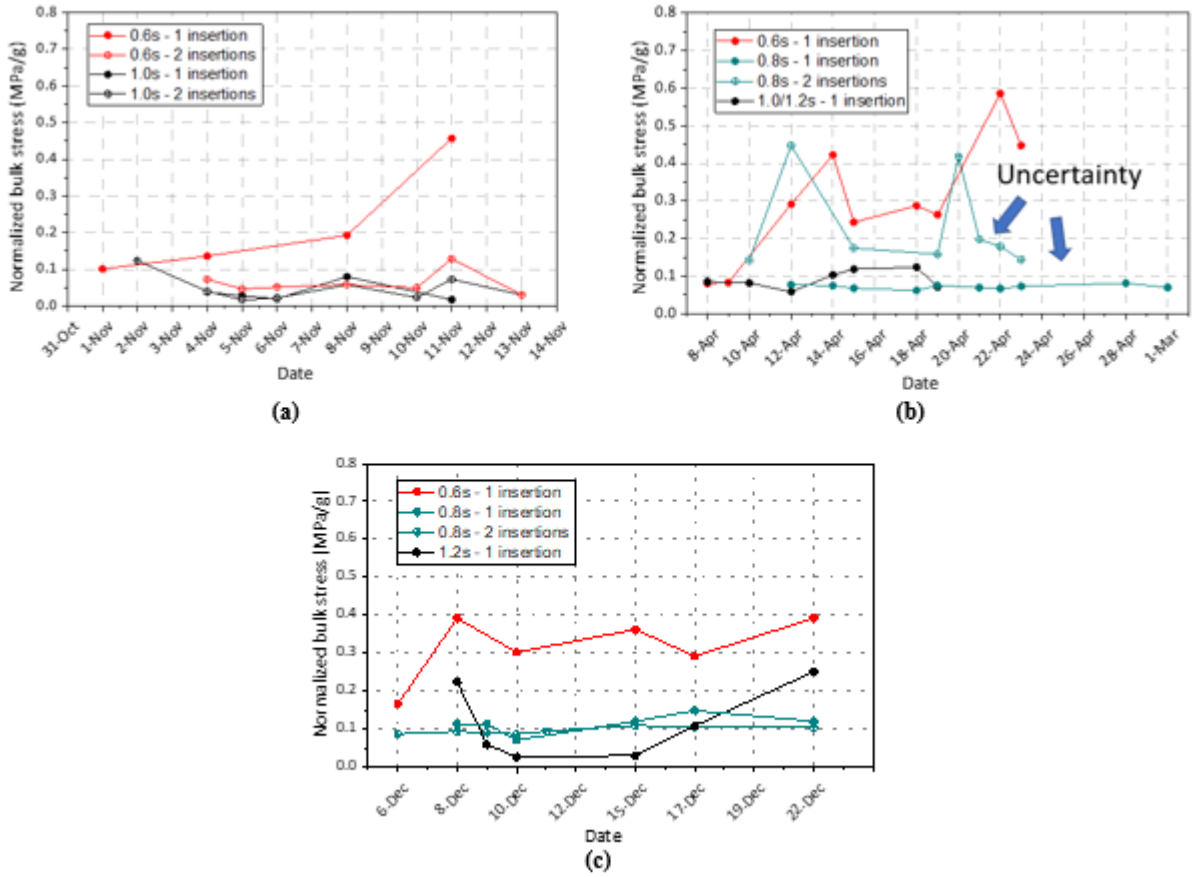

Figure 15. Comparison of normalized bulk stress: (a) Bellwood (clean ballast); (b) Tunnelhill (fouled ballast); (c) Chesapeake (clean ballast)

In the clean ballast scenarios (Figure 15 (a) and (c)), the normalized bulk stress remained relatively stable or exhibited a slight increase across most tamping conditions throughout the observation period. Notably, toward the end of the monitoring period, there was a significant rise in stress levels for the cases involving two insertions with a 0.6-second squeeze time. This sudden increase suggests a delayed compaction or settlement effect, where the ballast, after undergoing repeated tamping actions, achieved a more compact and stable state, thereby

enhancing its ability to resist applied stresses. In contrast, the conditions with a single insertion tend to show lower stress levels, indicating that multiple tamping passes may be more effective in achieving the desired compaction and long-term stability of the ballast.

On the other hand, the fouled ballast (Figure 15 (b)) displayed a more erratic and fluctuating pattern in normalized bulk stress. The stress levels varied significantly, particularly in the conditions involving two insertions at 0.8 seconds and a single insertion at longer squeeze times. The graph marks areas of "Uncertainty," highlighting these fluctuations, which may reflect the inconsistent response of fouled ballast to tamping. These irregular patterns could be attributed to the uneven distribution of fouling materials, which alters the mechanical properties of the ballast, making it more challenging to achieve uniform compaction. Unlike clean ballast, the fouled ballast does not exhibit a clear trend toward stabilization, suggesting that the presence of fouling materials impedes the ballast from reaching a compact state that supports sustained track performance.

4.3 Tamping Energy

The energy imparted to ballast particles by the tamping unit, which operates at a frequency of 35 Hz, plays a crucial role in determining the effectiveness of the tamping process and the subsequent stability of the track. When the tamping unit vibrates at this frequency, it generates a specific amount of energy that is transferred to the ballast particles, causing them to rearrange, compact, and interlock more effectively. The amount of energy received by the ballast particles directly influences the degree of compaction achieved, which in turn impacts the overall stability of the ballast layer.

By calculating the energy received by the ballast particles during tamping, engineers can gain valuable insights into the compaction process and predict the long-term stability of the track. This energy transfer is essential because it affects how well the ballast particles are packed together, reducing voids and creating a denser and more stable foundation for railway tracks. The received energy can be correlated with the normalized bulk stress, a key parameter that reflects the mechanical strength and load-bearing capacity of the ballast after tamping.

The average power spectrum depicted in Figure 16 provides a detailed analysis of the frequency distribution of energy during a tamping operation with two insertions over a 1-second duration. The plot reveals that most of the energy was concentrated in the 25-40 Hz frequency range, with particularly pronounced peaks around 30-35 Hz. These peaks are closely aligned with the operational frequency of the tamping unit, which operates at 35 Hz, indicating that the tamping unit is effectively transferring energy to the ballast at its intended frequency.

This concentration of energy at the target frequency suggests that the tamping unit was functioning as designed, delivering consistent vibrational energy that is crucial for achieving effective ballast compaction. The presence of two distinct peaks at around 2 and 4 seconds into the operation indicates the moments when the tamping force was most effectively applied, corresponding to the timing of the two insertions. These peaks highlight the intervals during which the ballast particles were likely undergoing the most significant reorientation and compaction due to the applied vibrational energy.

The color gradient in the plot, which ranges from blue (low energy) to yellow (high energy), shows that the energy distribution was not uniform across the frequency spectrum or over time. The highest energy levels, represented by yellow, are concentrated around the 35 Hz frequency

during the active tamping periods. This further confirms that the tamping process was predominantly effective at this frequency, which is critical for achieving the desired compaction and stability of the ballast. More energy plots are included in Appendix A.

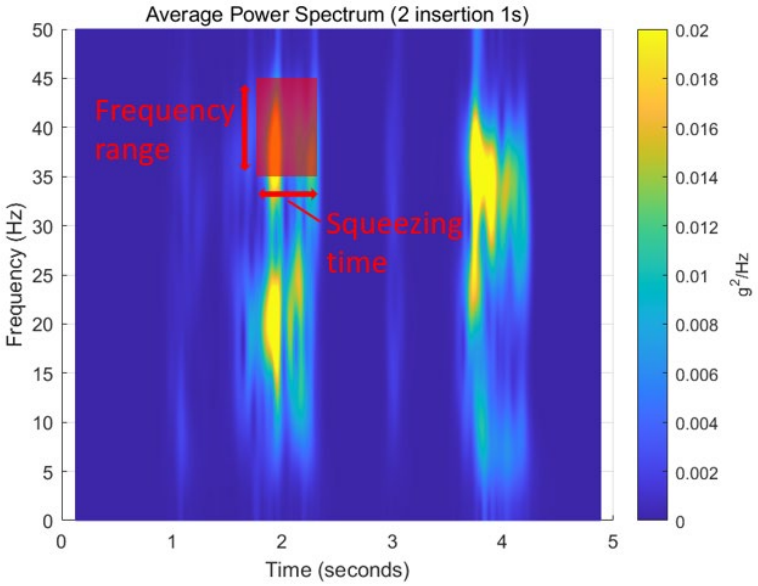

Figure 16 Average power spectrum of ballast acceleration from SmartRock sensors

The following equation is used to calculate the imparted energy to the ballast. This equation considers the energy density in the specific frequency range during the squeezing time. The frequency range was selected from 35Hz to 45Hz to be compatible with the cases where the vibration frequency reached up to 50Hz as needed.

$$dB_{tamping} = 10\log\left(\sum\sum^{Frequency\ range\ *Squeezing\ time}_{*Energy\ desity}\right)$$
$$= 10\log\left(\iint E(f,t)\,df\,dt\right)$$

Sample variances in different cases were calculated for normalized bulk stress. The following equation is used in statistics to measure the spread or dispersion of a set of bulk stress data points around the mean (i.e., average) of that data set:

$$S^2 = \frac{\sum(x_i - \bar{x})^2}{n-1}$$

Where S denotes bulk stress variances x_i represents bulk stress in a specific date. $\bar{x}$ is the sample mean, which is the average of all the data points in the sample. n is the number of data points in the sample.

Figure 17 presents a scatter plot that examines the relationship between tamping energy (measured in decibels, dB) and the normalized bulk stress variance for different tamping conditions across three sites: Site 1 (Bellwood) and Site 3 (Chesapeake), which have clean ballast, and Site 2 (Tunnelhill), which has fouled ballast. The data points represent different tamping scenarios, including various insertion counts and squeeze times, indicated by distinct markers for each site.

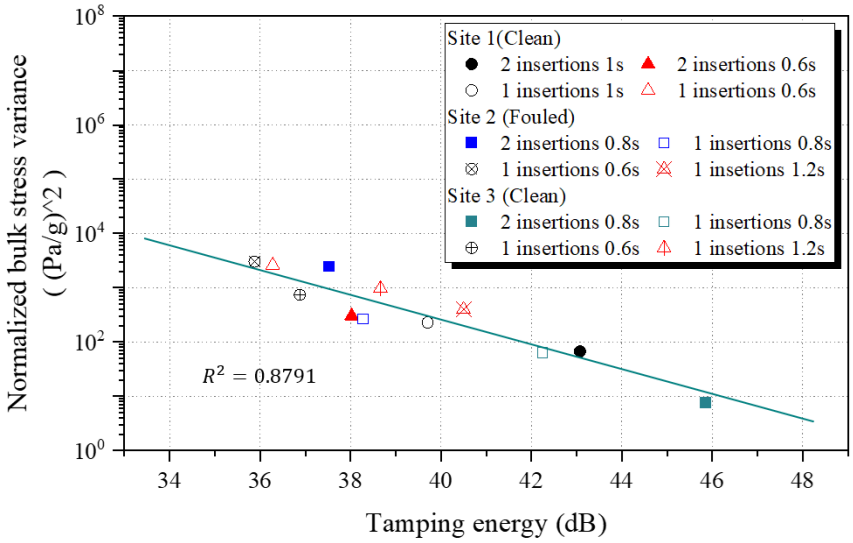

Figure 17 Relationship between tamping energy and normalized bulk stress variance

The plot shows a clear negative correlation between tamping energy and normalized bulk stress variance, as indicated by the downward-sloping trend line with a high R^2 value of 0.8791. This strong correlation suggests that as tamping energy increases, the variance in normalized bulk stress decreases. In other words, higher tamping energy results in more consistent and stable compaction of the ballast, as reflected by the lower variance in stress.

For Site 1 and Site 3, both with clean ballast, the data points generally fall along the trend line, indicating that higher tamping energy effectively reduces the stress variance. This is consistent with the expectation that clean ballast, when subjected to higher energy tamping, achieves better compaction, leading to more uniform stress distribution. The data from these sites suggest that both one and two insertions with various squeeze times contribute to this improved stability, although higher energy tamping tends to yield better results.

In contrast, the data from Site 2, which has fouled ballast, shows more variability. Although the fouled ballast still follows the general trend of decreasing stress variance with increasing tamping energy, the data points are more scattered compared to those from the clean ballast sites. This indicates that while higher tamping energy can still reduce stress variance in fouled ballast, the effectiveness is less consistent. The presence of fouling materials likely interferes with the compaction process, leading to less predictable outcomes.

Overall, this analysis underscores the importance of sufficient tamping energy in achieving stable ballast compaction. The strong correlation between tamping energy and stress variance suggests that higher energy tamping is important for minimizing stress variability and enhancing track stability, especially in clean ballast conditions. However, the variability observed in fouled ballast highlights the challenges in achieving similar levels of stability, suggesting a need for tailored tamping strategies or additional maintenance in such conditions.

4.4 Tamper-ballast Interaction

Figure 18 compares the tamper reaction force and ballast bulk stress in two different tamping cases: one with a 0.6-second squeezing time and one insertion (Figure 18 (a)), and another with a 0.8-second squeezing time and one insertion (Figure 18 (b)). The plots are divided into two

sections for each case: the top half shows the ballast bulk stress (measured in MPa), while the bottom half illustrates the cylinder pressure exerted by the tamper tool (expressed as a percentage of the maximum force).

In both cases, the bulk stress represents how effectively the ballast was compacted during tamping. For the 0.8-second squeezing time (Figure 18 (b)), the bulk stress shows a more stable and consistent response compared to the 0.6-second squeezing time (Figure 18 (a)). The peaks and drops in the 0.6-second scenario suggest that shorter squeezing time leads to rapid energy transfer, which might result in less uniform compaction and potentially lower overall ballast stability.

Figure 18 (b) shows that for the 0.8-second squeezing time, the bulk stress behaved differently. There are more fluctuations and less pronounced peaks in the stress readings, indicating that the interaction between the tamper tool and the ballast was less stable in this case. The stress pattern shows several dips, which may suggest moments where the ballast resettled or exhibited uneven resistance to the tamping forces. The reaction force (lower half of Figure 18 (b)) shows a more consistent build-up of force during the squeezing phase but with greater variability and more pronounced oscillations than in the 0.6-second case.

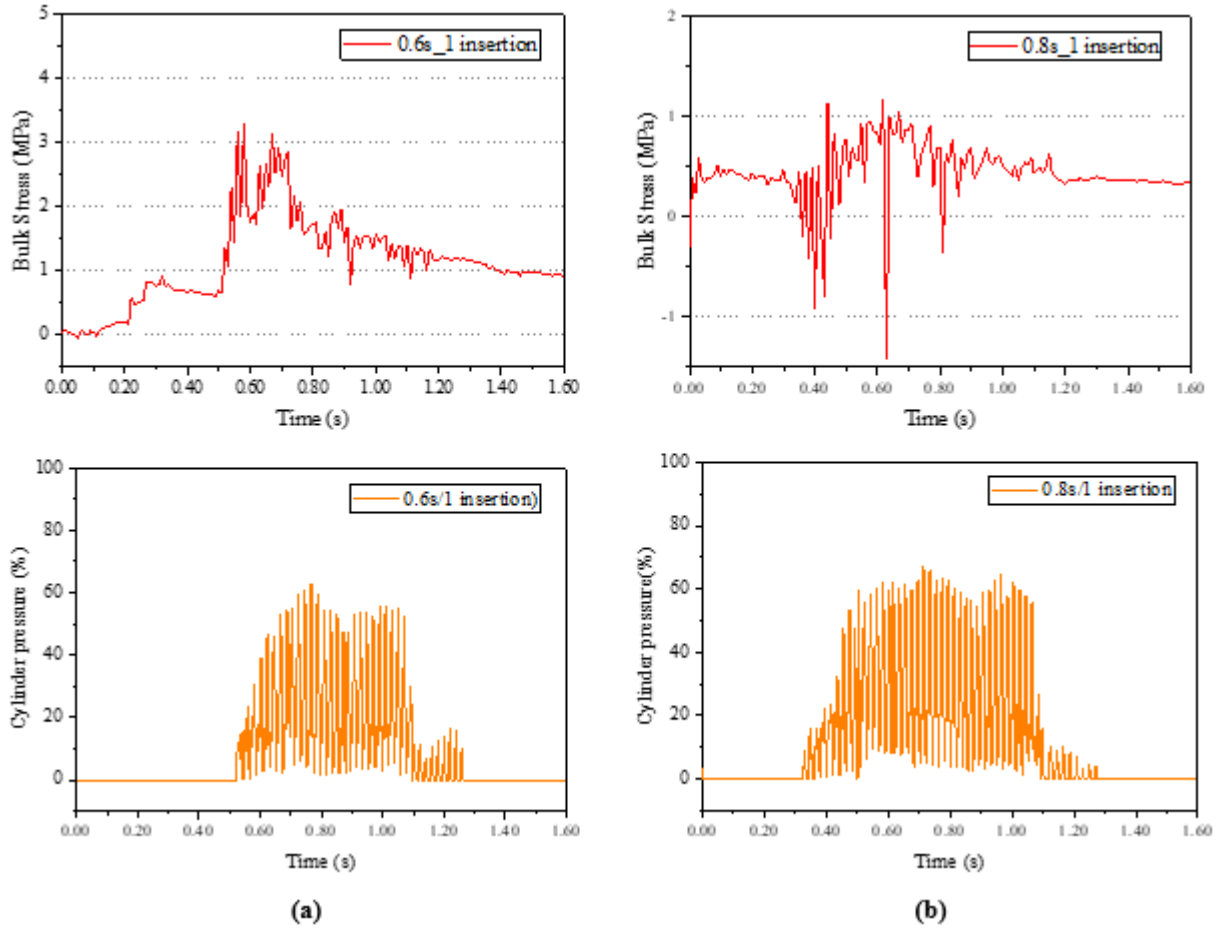

Figure 18 Tamper reaction force and ballast bulk stress: (a) 0.6s squeezing time and one insertion; (b) 0.8s squeezing time and one insertion

Figure 19 provides a comparison of tamper tine displacement and ballast bulk stress during tamping operations with two different cases: a 0.6-second squeezing time and one insertion (Figure 19 (a)), and a 0.8-second squeezing time and one insertion (Figure 19 (b)). The tamper tine displacement reflects the movement of the tamping tool during the squeezing phase. In both cases, the tamper tine follows a predictable trajectory, reaching a maximum displacement before retracting. However, the 0.8-second squeezing time (Figure 19 (b)) shows a smoother and more gradual displacement curve, indicating a steadier and more efficient tamping process. This controlled displacement suggests that the tamping tools were applying consistent pressure over a longer duration, which likely resulted in better consolidation of the ballast particles. In contrast, the 0.6-second squeezing time (Figure 19 (a)) shows a more rapid increase and sharper changes in displacement, suggesting that a shorter squeeze may be less effective in uniformly compacting the ballast.

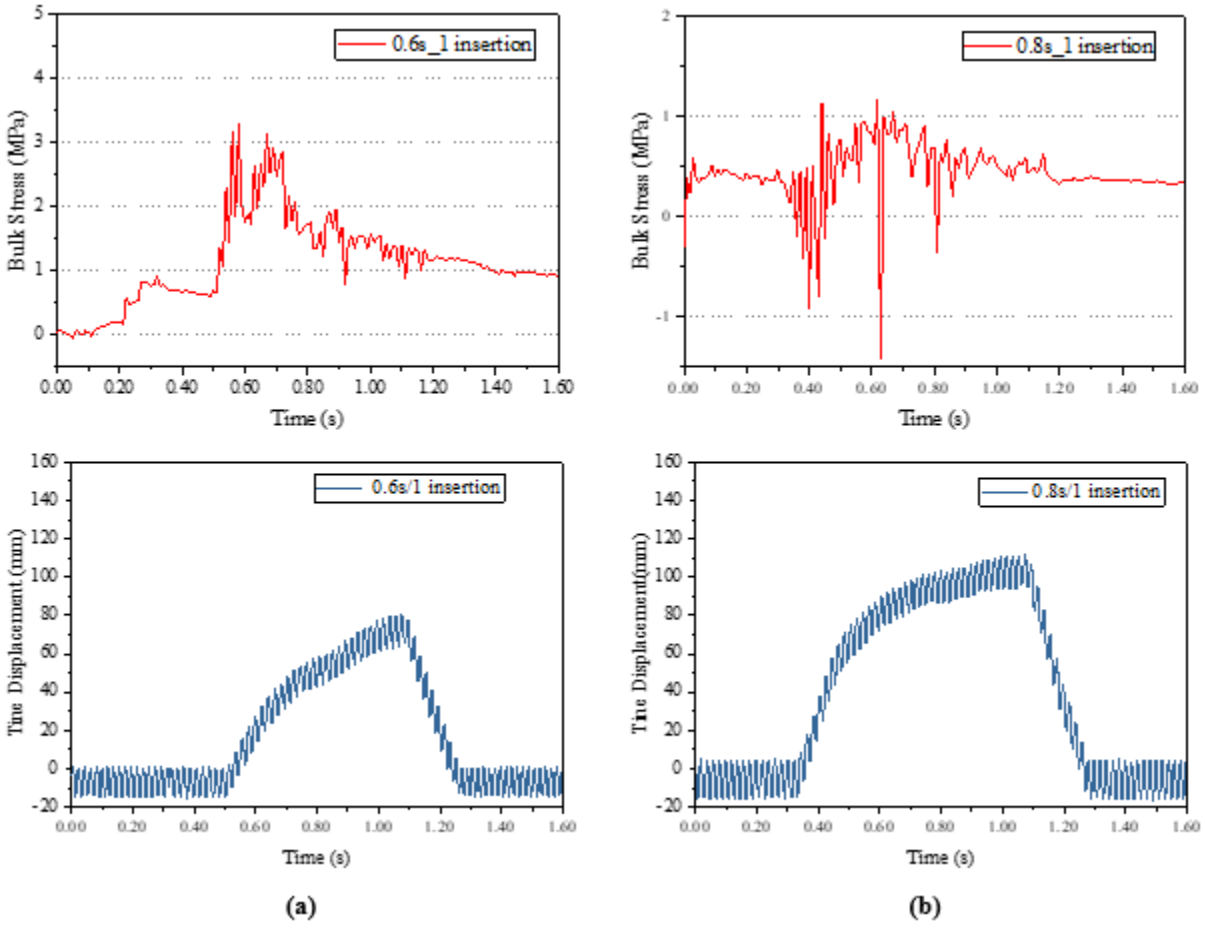

Figure 19. Tamper tine displacement and ballast bulk stress: (a) 0.6s squeezing time and one insertion; (b) 0.8s squeezing time and one insertion

5. Conclusion

This study highlights the crucial role that tamping parameters (e.g., the number of insertions and squeezing time) play in the effectiveness of ballast compaction and overall track stability. Field tests demonstrated that tamping efficiency can be significantly improved by adjusting these parameters. Proper optimization of tamping practices, particularly in terms of squeezing duration, can lead to more effective ballast consolidation, improved load distribution, and reduced track settlement over time. The findings suggest that using a longer squeeze time leads to better overall performance compared to shorter tamping cycles.

A clear distinction was observed in how clean and fouled ballast respond to tamping operations. Clean ballast showed a more favorable response to tamping, with smoother, more effective energy transfer and particle reorientation. This resulted in greater compaction efficiency, as clean ballast particles can shift and compact more easily when not obstructed by fouling materials. Conversely, fouled ballast posed a challenge to tamping operations, as the presence of contaminants such as dirt and debris impeded the transmission of tamping forces. This led to less efficient compaction and an increased need for more intensive tamping strategies to achieve the same level of stability as with clean ballast.

The energy analysis conducted during the tamping process underscores the importance of energy transfer in evaluating ballast stability. The use of SmartRock sensors allowed for real-time monitoring of how much energy was absorbed by the ballast during tamping. In clean ballast, the energy applied was used more efficiently, leading to better compaction and more stable track conditions. In contrast, fouled ballast exhibited higher energy losses due to the interference of fouling materials, reducing the effectiveness of the tamping process. This highlights the potential for energy monitoring as a reliable indicator of ballast condition and the success of tamping operations.

The application of SmartRock sensors in this study proved to be a highly effective tool for capturing the dynamic behavior of ballast during tamping. These sensors are reuseable and provide valuable data on particle movement, stress changes, and energy absorption, offering deeper insights into the mechanical interactions between the tamping tools and the ballast. The real-time data collection made it possible to observe how different tamping parameters affected ballast stability. Given their utility, SmartRock sensors can be further integrated into regular railway maintenance practices to monitor ballast condition and adjust tamping operations more effectively.

In conclusion, this study underscores the importance of fine-tuning tamping parameters to suit varying ballast conditions. This research demonstrates that by adopting a more data-driven approach – leveraging advanced sensor technology like SmartRock and focusing on energy transfer – railway operators can optimize tamping operations to enhance track stability and longevity. These improvements will not only increase the efficiency of maintenance practices but also contribute to safer, more reliable railway operations.

Future work should focus on the relationship between ballast stability and particle bulk stress change by incorporating advanced numerical solutions, such as the Discrete Element Method. Moreover, effective tamping energy will be connected to the data from the tamper instead of SmartRock data.

6. References

Audley, M., & Andrews, J. (2013). The effects of tamping on railway track geometry degradation. *Proceedings of the Institution of Mechanical Engineers, Part F: Journal of Rail and Rapid Transit*, *227*(4), 376–391.

Guo, Y., Markine, V., & Jing, G. (2021). Review of ballast track tamping: Mechanism, challenges and solutions. *Construction and Building Materials*, *300*, 123940.

Huang, H., Liu, S., & Qiu, T. (2018). Identification of Railroad Ballast Fouling through Particle Movements. *Journal of Geotechnical and Geoenvironmental Engineering*, *144*(4), 02818001.

Liu, S., Gao, Y., & Huang, H. (2017). Evaluating Ballast Migration on Curved Track Using "SmartRock." *2017 American Railway Engineering and Maintenance-of-Way Association (AREMA)*.

Liu, S., Huang, H., & Qiu, T. (2015). Laboratory Development and Testing of SmartRock for Railroad Ballast Using Discrete Element Modeling. *2015 Joint Rail Conference*, V001T01A019.

Liu, S., Huang, H., & Qiu, T. (2017). Behavior of Geogrid-Reinforced Railroad Ballast Particles Under Different Loading Configurations During Initial Compaction Phase. *2017 Joint Rail Conference*, V001T01A002.

Liu, S., Huang, H., Qiu, T., & Gao, L. (2017). Comparison of Laboratory Testing Using SmartRock and Discrete Element Modeling of Ballast Particle Movement. *Journal of Materials in Civil Engineering*, *29*(3), D6016001.

Liu, S., Huang, H., Qiu, T., & Kerchof, B. (2019). Characterization of Ballast Particle Movement at Mud Spot. *Journal of Materials in Civil Engineering*, *31*(1), 04018339.

Liu, S., Huang, H., Qiu, T., & Kwon, J. (2016). Effect of geogrid on railroad ballast particle movement. *Transportation Geotechnics*, *9*, 110–122.

Liu, S., Huang, H., Qiu, T., & Kwon, J. (2017). Comparative Evaluation of Particle Movement in a Ballast Track Structure Stabilized with Biaxial and Multiaxial Geogrids. *Transportation Research Record: Journal of the Transportation Research Board*, *2607*(1), 15–23.

Liu, S., Huang, H., Qiu, T., & Shen, S. (2018). Sensing Mechanism and Real-Time Computing for Granular Materials. *Journal of Computing in Civil Engineering*, *32*(4), 04018023.

Liu, S., Qiu, T., Qian, Y., Huang, H., Tutumluer, E., & Shen, S. (2019). Simulations of large-scale triaxial shear tests on ballast aggregates using sensing mechanism and real-time (SMART) computing. *Computers and Geotechnics*, *110*, 184–198.

Tutumluer, E., Huang, H., Hashash, Y., & Ghaboussi, J. (2006). *Aggregate Shape Effects on Ballast Tamping and Railroad Track Lateral Stability*. 23.

Zeng, K., Huang, H., & Song, S. (2020). Displacement Measurement Based on Data Fusion and Real-Time Computing. *Journal of Performance of Constructed Facilities*, *34*(6), 04020118.

Zeng, K., Nazari, S., Zhou, Y., Wallace, J., & Huang, H. (2024). Investigation into the effect of railroad ballast fouling on the ballast movements and strain change using "SmartGrid." *Transportation Geotechnics*, *48*, 101307.

Zeng, K., Qiu, T., Bian, X., Xiao, M., & Huang, H. (2019). Identification of ballast condition using SmartRock and pattern recognition. *Construction and Building Materials*, *221*, 50-59.

Zhou, Y., Schlake, B., Hansmann, F., Huang, H., Antony, B., Zeng, K., & Zhang, C. (2024). Particle Motion and Stress Response Interacted with Machine Activity: Railroad Tamping Strategy. *Transportation Geotechnics*, 101188.

Appendix A.
Tamping Energy Plot

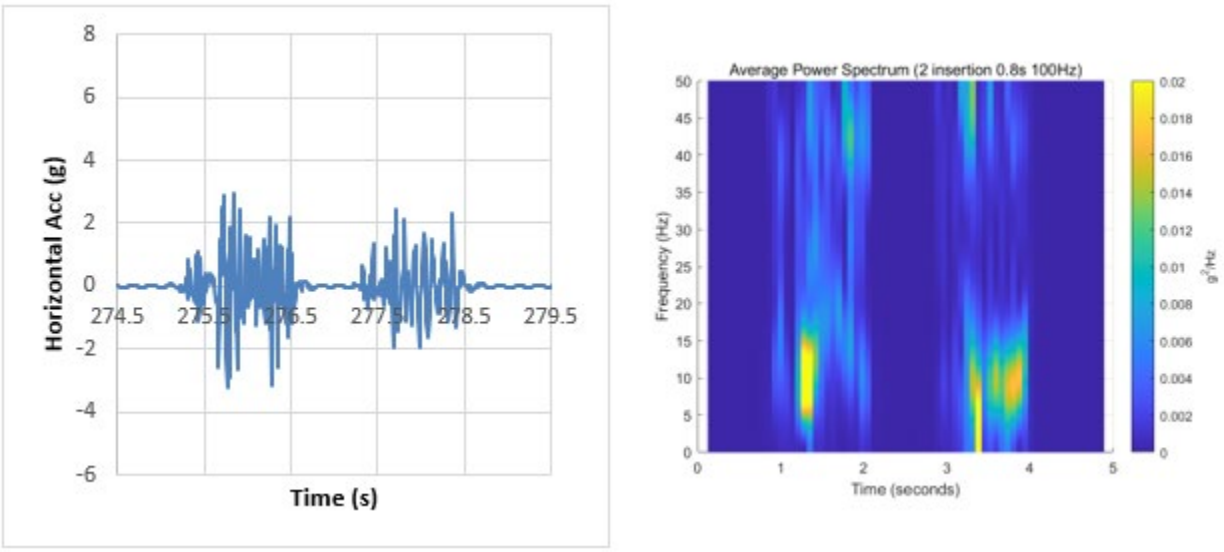

Figure A.1 Average power spectrum in case of two insertions 0.8s for fouled ballast

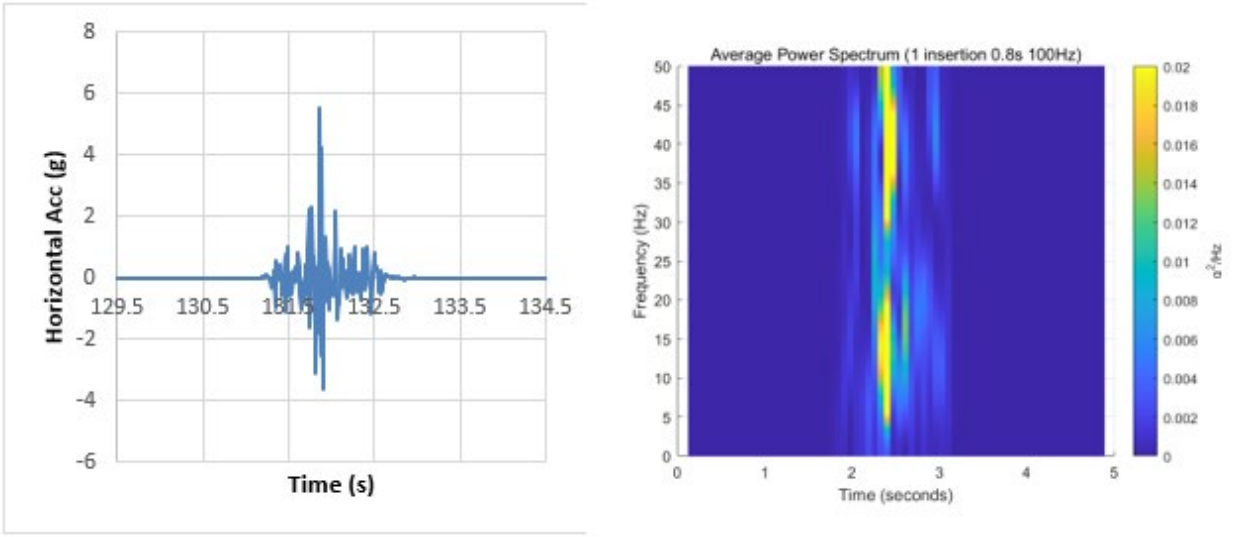

Figure A.2 Average power spectrum in case of one insertion 0.8s for fouled ballast

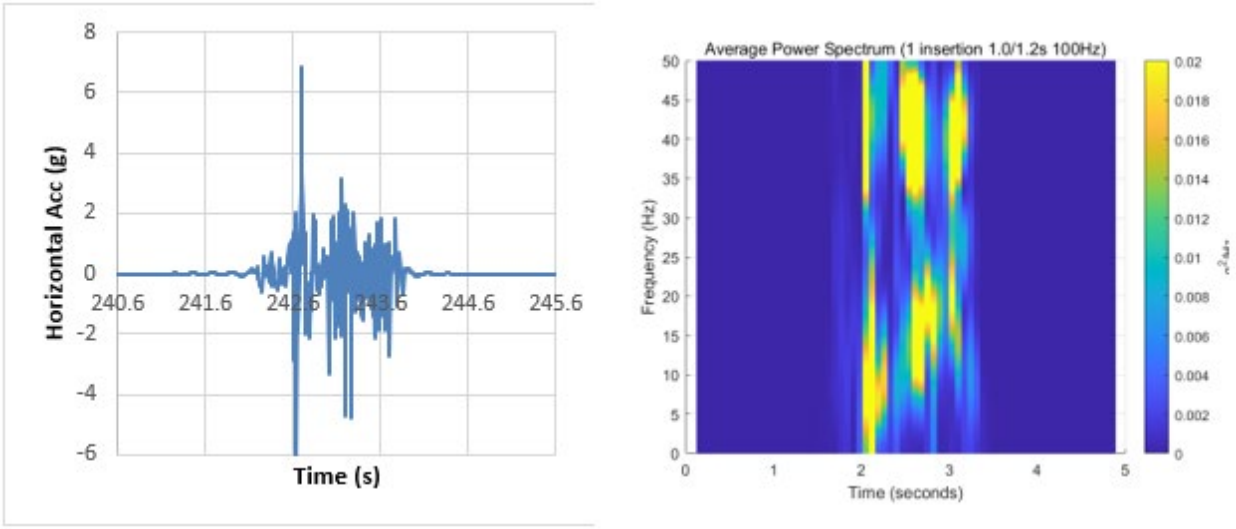

Figure A.3 Average power spectrum in case of one insertion 1.2s for fouled ballast

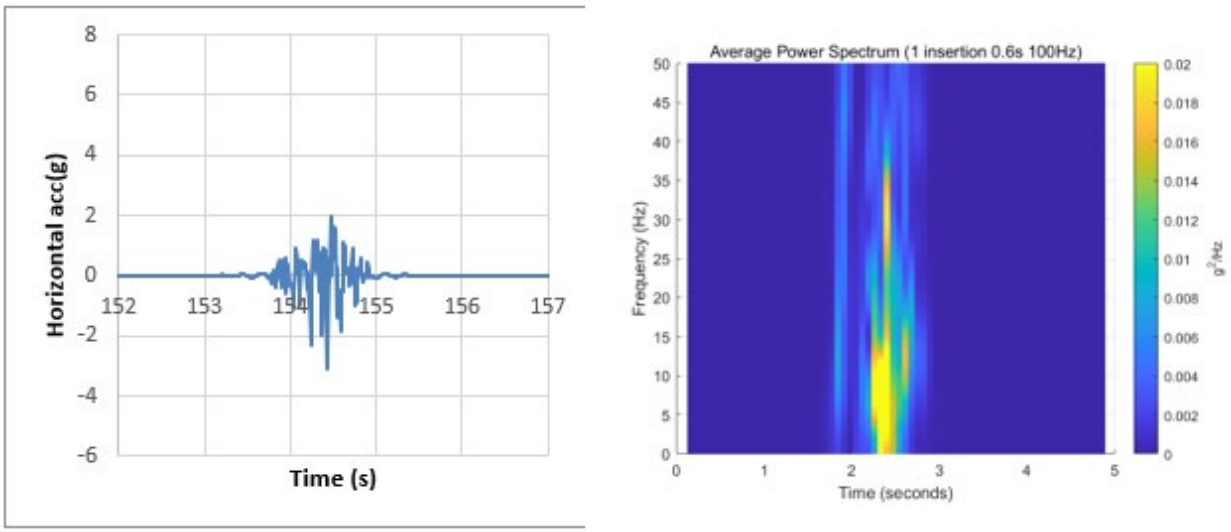

Figure A.4 Average power spectrum in case of one insertion 0.6s for fouled ballast

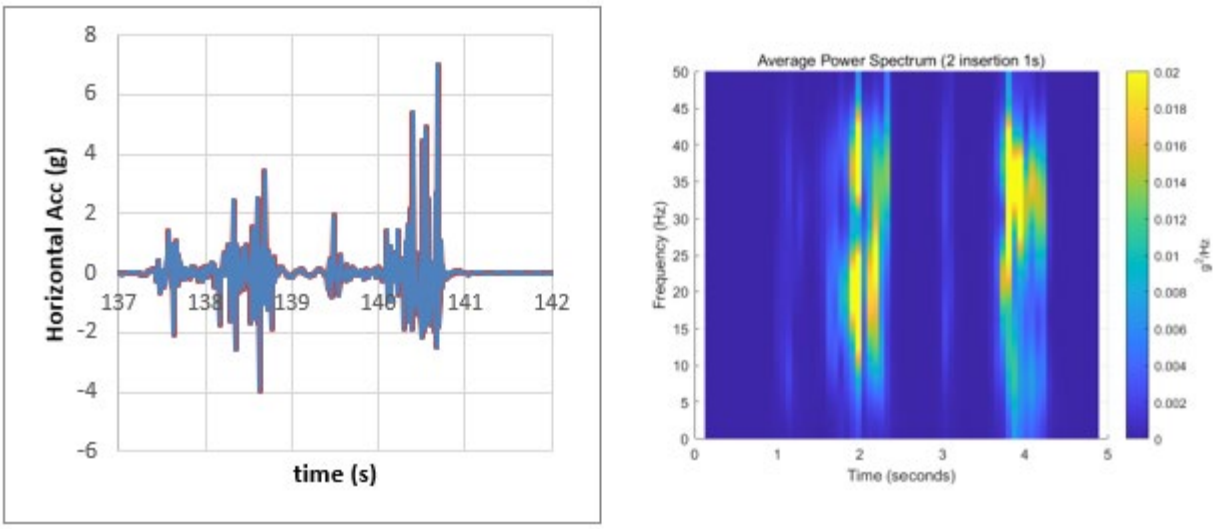

Figure A.5 Average power spectrum in case of two insertions 1.0s for clean ballast

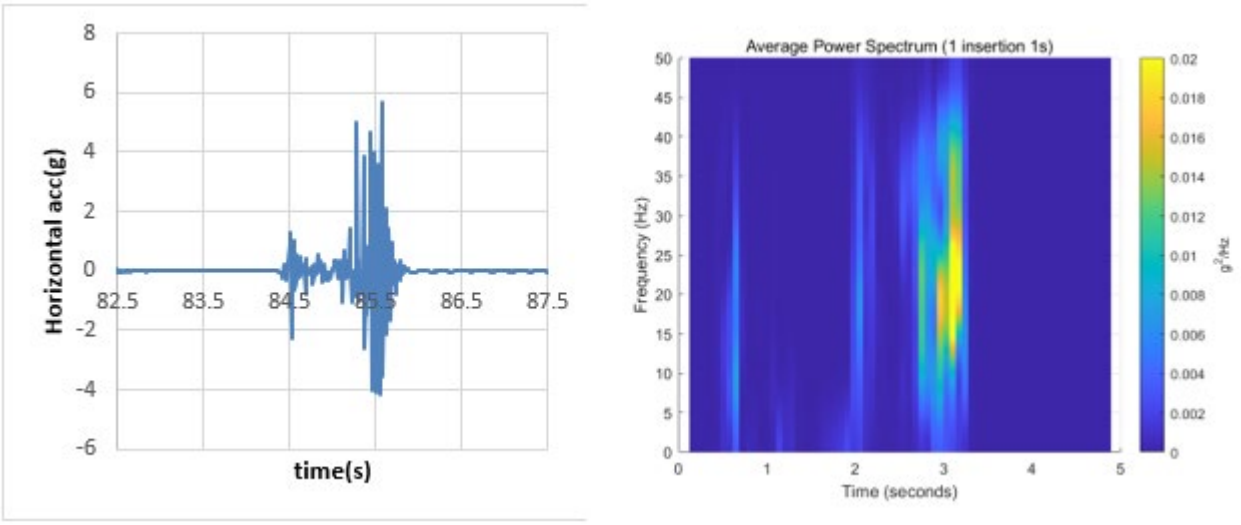

Figure A.6 Average power spectrum in case of one insertion 1.0s for clean ballast

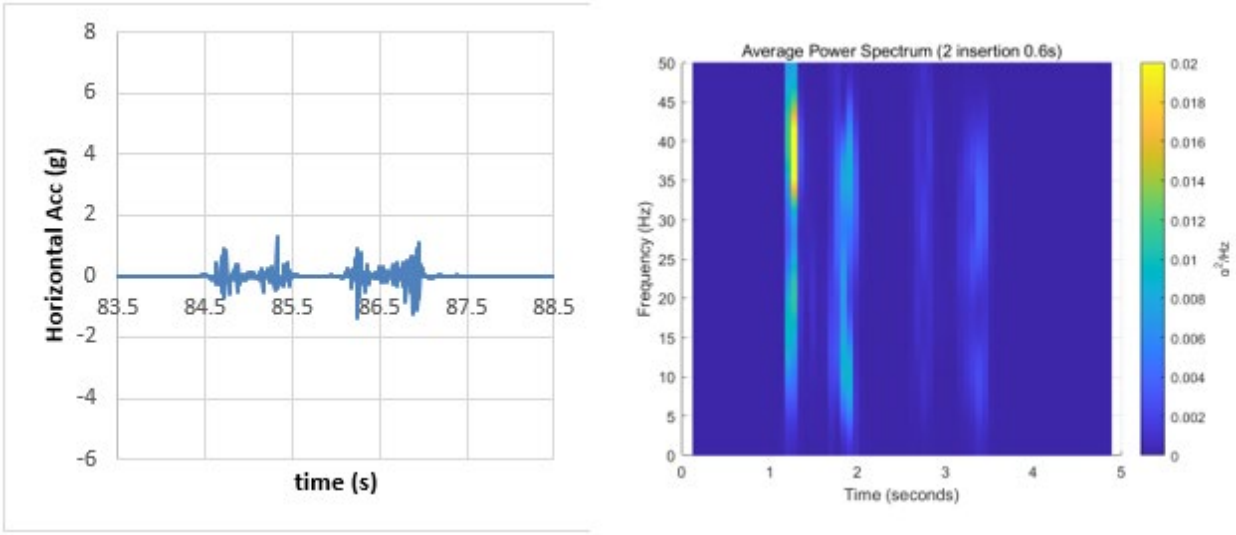

Figure A.7 Average power spectrum in case of two insertions 0.6s for clean ballast

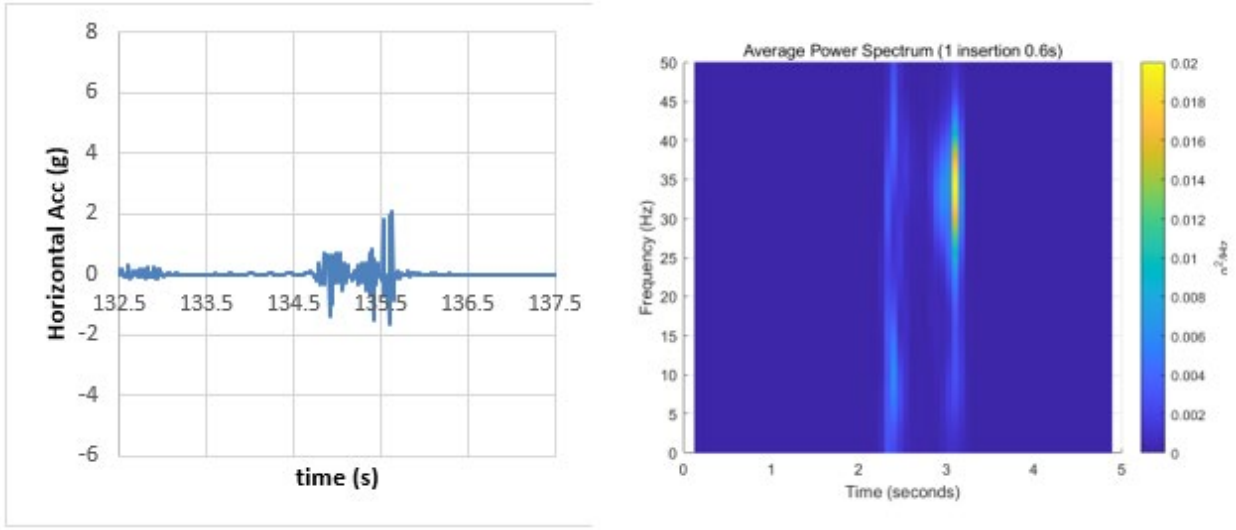

Figure A.8 Average power spectrum in case of one insertion 0.6s for clean ballast

Appendix B.
MATLAB code for SmartRock data analysis

```
tic
clc
clear
filelo = file path;
%% com1
for i = 1 : 6
   SRT1(i).label = '2inst 1s';
   %acc
   SRT1(i).accdata = csvread([filelo,'computer
1\SR0',num2str(i),'\tamping\11_03_Accel.csv'],1,2);
   SRT1(i).acc(:,2:4) = bsxfun(@minus, SRT1(i).accdata(:,1:3), SRT1(i).accdata(1,1:3));
%     SRT1(i).acc(:,2:4) = SRT1(i).accdata(:,1:3);
   SRT1(i).acc(:,2:4) =
highpass(SRT1(i).acc(:,2:4),0.1,'Steepness',0.85,'StopbandAttenuation',60);
   SRT1(i).acc(:,5) = ( SRT1(i).acc(:,2).^2 + SRT1(i).acc(:,3).^2 ).^0.5;%horizontal acc value
   SRT1(i).acc(:,6) = ( SRT1(i).acc(:,2).^2 + SRT1(i).acc(:,3).^2 +
SRT1(i).acc(:,4).^2).^0.5;%all acc value


   h = 13;m = 34;
   for j = 1:length(SRT1(i).accdata(:,1))
      if j == 1
         SRT1(i).acc(j,1) = SRT1(i).accdata(j,9)/1000 + SRT1(i).accdata(j,8)+
(SRT1(i).accdata(j,7) - m) * 60 + (SRT1(i).accdata(j,6) - h) * 3600;
      else
         SRT1(i).acc(j,1) = (SRT1(i).accdata(j,9) - SRT1(i).accdata(j-1,9))/1000 +
SRT1(i).accdata(j,8) - SRT1(i).accdata(j-1,8) + (SRT1(i).accdata(j,7) - SRT1(i).accdata(j-1,7)) *
60 + (SRT1(i).accdata(j,6) - SRT1(i).accdata(j-1,6)) * 3600 + SRT1(i).acc(j-1,1);
      end
   end
   SRT1(i).acc(:,1) = SRT1(i).acc(:,1) - SRT1(i).acc(1,1);
   [SRT1(i).reacc(:,2:4),SRT1(i).reacc(:,1)] = resample(SRT1(i).acc(:,2:4),SRT1(i).acc(:,1),100);
```

```
   SRT1(i).reacc(:,5) = ( SRT1(i).reacc(:,2).^2 + SRT1(i).reacc(:,3).^2 ).^0.5;%horizontal acc
value
   SRT1(i).reacc(:,6) = ( SRT1(i).reacc(:,2).^2 + SRT1(i).reacc(:,3).^2 + SRT1(i).reacc(:,4).^2
).^0.5;%all acc value


   %eul
   SRT1(i).quat = csvread([filelo,'computer
1\SR0',num2str(i),'\tamping\11_03_Quaternion.csv'],1,2);
   SRT1(i).eul(:,2:4) = quat2eul(SRT1(i).quat(:,1:4));
   SRT1(i).eul(:,2:4) = bsxfun(@minus, SRT1(i).eul(:,2:4), SRT1(i).eul(1,2:4));
   SRT1(i).eul(:,2:4) = bsxfun(@times, SRT1(i).eul(:,2:4), 180/pi);
   for j = 1:length(SRT1(i).quat(:,1))
      if j == 1
         SRT1(i).eul(j,1) = SRT1(i).quat(j,10)/1000 + SRT1(i).quat(j,9)+ (SRT1(i).quat(j,8) - m)
* 60 + (SRT1(i).quat(j,7) - h) * 3600;
      else
         SRT1(i).eul(j,1) = (SRT1(i).quat(j,10) - SRT1(i).quat(j-1,10))/1000 + SRT1(i).quat(j,9) -
SRT1(i).quat(j-1,9) + (SRT1(i).quat(j,8) - SRT1(i).quat(j-1,8)) * 60 + (SRT1(i).quat(j,7) -
SRT1(i).quat(j-1,7)) * 3600 + SRT1(i).eul(j-1,1);
      end
   end
   SRT1(i).eul(:,1) = SRT1(i).eul(:,1) - SRT1(i).eul(1,1);
   [SRT1(i).reeul(:,2:4),SRT1(i).reeul(:,1)] = resample(SRT1(i).eul(:,2:4),SRT1(i).eul(:,1),100);



   %pressure
   SRT1(i).voltage = csvread([filelo,'computer
1\SR0',num2str(i),'\tamping\11_03_Pressure.csv'],1,2);
   SRcoff1{i} = csvread([filelo,'computer 1\SR0',num2str(i),'\params.csv'],1,1);


   initvoltage(1) = mean(SRT1(i).voltage(1:100,1));
   initvoltage(2) = mean(SRT1(i).voltage(1:100,2));
   initvoltage(3) = mean(SRT1(i).voltage(1:100,3));
```

```
   SRT1(i).pressure(:,2) = (initvoltage(1) - SRT1(i).voltage(:,1)) .* SRcoff1{i}(2,1);% -
SRcoff1{i}(2,2) .* log(25) + SRcoff1{i}(2,3);x
   SRT1(i).pressure(:,3) = (initvoltage(2) - SRT1(i).voltage(:,2)) .* SRcoff1{i}(3,1);% -
SRcoff1{i}(3,2) .* log(25) + SRcoff1{i}(3,3);y
   SRT1(i).pressure(:,4) = (initvoltage(3) - SRT1(i).voltage(:,3)) .* SRcoff1{i}(1,1);% -
SRcoff1{i}(1,2) .* log(25) + SRcoff1{i}(1,3);z
   SRT1(i).pressure(:,5) = SRT1(i).pressure(:,2) + SRT1(i).pressure(:,3) + SRT1(i).pressure(:,4);


   for j = 1:length(SRT1(i).voltage(:,1))
     if j == 1
        SRT1(i).pressure(j,1) = SRT1(i).voltage(j,9)/1000 + SRT1(i).voltage(j,8)+
(SRT1(i).voltage(j,7) - m) * 60 + (SRT1(i).voltage(j,6) - h) * 3600;
     else
        SRT1(i).pressure(j,1) = (SRT1(i).voltage(j,9) - SRT1(i).voltage(j-1,9))/1000 +
SRT1(i).voltage(j,8) - SRT1(i).voltage(j-1,8) + (SRT1(i).voltage(j,7) - SRT1(i).voltage(j-1,7)) *
60 + (SRT1(i).voltage(j,6) - SRT1(i).voltage(j-1,6)) * 3600 + SRT1(i).pressure(j-1,1);
     end
   end
   SRT1(i).pressure(:,1) = SRT1(i).pressure(:,1) - SRT1(i).pressure(1,1);
   [SRT1(i).repressure(:,2:4),SRT1(i).repressure(:,1)] =
resample(SRT1(i).pressure(:,2:4),SRT1(i).pressure(:,1),100);
   SRT1(i).repressure(:,5) = SRT1(i).repressure(:,2) + SRT1(i).repressure(:,3) +
SRT1(i).repressure(:,4);
end


%% com2
for i = [7 : 9,11]
   SRT1(i).label = '2inst 0.6s';
   %acc
   SRT1(i).accdata = csvread([filelo,'computer
2\SR',num2str(i),'\tamping\11_03_Accel.csv'],1,2);
   SRT1(i).acc(:,2:4) = bsxfun(@minus, SRT1(i).accdata(:,1:3), SRT1(i).accdata(1,1:3));
   SRT1(i).acc(:,2:4) =
highpass(SRT1(i).acc(:,2:4),0.1,'Steepness',0.85,'StopbandAttenuation',60);
   SRT1(i).acc(:,5) = ( SRT1(i).acc(:,2).^2 + SRT1(i).acc(:,3).^2 ).^0.5;%horizontal acc value
```

```
    SRT1(i).acc(:,6) = ( SRT1(i).acc(:,2).^2 + SRT1(i).acc(:,3).^2 + SRT1(i).acc(:,4).^2
).^0.5;%all acc value



    h = 13;m = 32;
    for j = 1:length(SRT1(i).accdata(:,1))
        if j == 1
            SRT1(i).acc(j,1) = SRT1(i).accdata(j,9)/1000 + SRT1(i).accdata(j,8)+
(SRT1(i).accdata(j,7) - m) * 60 + (SRT1(i).accdata(j,6) - h) * 3600;
        else
            SRT1(i).acc(j,1) = (SRT1(i).accdata(j,9) - SRT1(i).accdata(j-1,9))/1000 +
SRT1(i).accdata(j,8) - SRT1(i).accdata(j-1,8) + (SRT1(i).accdata(j,7) - SRT1(i).accdata(j-1,7)) *
60 + (SRT1(i).accdata(j,6) - SRT1(i).accdata(j-1,6)) * 3600 + SRT1(i).acc(j-1,1);
        end
    end
    SRT1(i).acc(:,1) = SRT1(i).acc(:,1) - SRT1(i).acc(1,1);
    [SRT1(i).reacc(:,2:4),SRT1(i).reacc(:,1)] = resample(SRT1(i).acc(:,2:4),SRT1(i).acc(:,1),100);
    SRT1(i).reacc(:,5) = ( SRT1(i).reacc(:,2).^2 + SRT1(i).reacc(:,3).^2 ).^0.5;%horizontal acc
value
    SRT1(i).reacc(:,6) = ( SRT1(i).reacc(:,2).^2 + SRT1(i).reacc(:,3).^2 + SRT1(i).reacc(:,4).^2
).^0.5;%all acc value


    %eul
    SRT1(i).quat = csvread([filelo,'computer
2\SR',num2str(i),'\tamping\11_03_Quaternion.csv'],1,2);
    SRT1(i).eul(:,2:4) = quat2eul(SRT1(i).quat(:,1:4));
    SRT1(i).eul(:,2:4) = bsxfun(@minus, SRT1(i).eul(:,2:4), SRT1(i).eul(1,2:4));
    SRT1(i).eul(:,2:4) = bsxfun(@times, SRT1(i).eul(:,2:4), 180/pi);
    for j = 1:length(SRT1(i).quat(:,1))
        if j == 1
            SRT1(i).eul(j,1) = SRT1(i).quat(j,10)/1000 + SRT1(i).quat(j,9)+ (SRT1(i).quat(j,8) - m)
* 60 + (SRT1(i).quat(j,7) - h) * 3600;
        else
            SRT1(i).eul(j,1) = (SRT1(i).quat(j,10) - SRT1(i).quat(j-1,10))/1000 + SRT1(i).quat(j,9) -
SRT1(i).quat(j-1,9) + (SRT1(i).quat(j,8) - SRT1(i).quat(j-1,8)) * 60 + (SRT1(i).quat(j,7) -
SRT1(i).quat(j-1,7)) * 3600 + SRT1(i).eul(j-1,1);
```

```
    end
  end
  SRT1(i).eul(:,1) = SRT1(i).eul(:,1) - SRT1(i).eul(1,1);
  [SRT1(i).reeul(:,2:4),SRT1(i).reeul(:,1)] = resample(SRT1(i).eul(:,2:4),SRT1(i).eul(:,1),100);


  %pressure
  SRT1(i).voltage = csvread([filelo,'computer
2\SR',num2str(i),'\tamping\11_03_Pressure.csv'],1,2);
  SRcoff1{i} = csvread([filelo,'computer 2\SR',num2str(i),'\params.csv'],1,1);


  initvoltage(1) = mean(SRT1(i).voltage(1:100,1));
  initvoltage(2) = mean(SRT1(i).voltage(1:100,2));
  initvoltage(3) = mean(SRT1(i).voltage(1:100,3));


  SRT1(i).pressure(:,2) = (initvoltage(1) - SRT1(i).voltage(:,1)) .* SRcoff1{i}(2,1);% -
SRcoff1{i}(2,2) .* log(25) + SRcoff1{i}(2,3);
  SRT1(i).pressure(:,3) = (initvoltage(2) - SRT1(i).voltage(:,2)) .* SRcoff1{i}(3,1);% -
SRcoff1{i}(3,2) .* log(25) + SRcoff1{i}(3,3);
  SRT1(i).pressure(:,4) = (initvoltage(3) - SRT1(i).voltage(:,3)) .* SRcoff1{i}(1,1);% -
SRcoff1{i}(1,2) .* log(25) + SRcoff1{i}(1,3);
  SRT1(i).pressure(:,5) = SRT1(i).pressure(:,2) + SRT1(i).pressure(:,3) + SRT1(i).pressure(:,4);


  for j = 1:length(SRT1(i).voltage(:,1))
    if j == 1
      SRT1(i).pressure(j,1) = SRT1(i).voltage(j,9)/1000 + SRT1(i).voltage(j,8)+
(SRT1(i).voltage(j,7) - m) * 60 + (SRT1(i).voltage(j,6) - h) * 3600;
    else
      SRT1(i).pressure(j,1) = (SRT1(i).voltage(j,9) - SRT1(i).voltage(j-1,9))/1000 +
SRT1(i).voltage(j,8) - SRT1(i).voltage(j-1,8) + (SRT1(i).voltage(j,7) - SRT1(i).voltage(j-1,7)) *
60 + (SRT1(i).voltage(j,6) - SRT1(i).voltage(j-1,6)) * 3600 + SRT1(i).pressure(j-1,1);
    end
  end
  SRT1(i).pressure(:,1) = SRT1(i).pressure(:,1) - SRT1(i).pressure(1,1);
  [SRT1(i).repressure(:,2:4),SRT1(i).repressure(:,1)] =
resample(SRT1(i).pressure(:,2:4),SRT1(i).pressure(:,1),100);
```

```
   SRT1(i).repressure(:,5) = SRT1(i).repressure(:,2) + SRT1(i).repressure(:,3) +
SRT1(i).repressure(:,4);
end


%% com3
for i = [14,16,17,18]
   SRT1(i).label = '1inst 1s';
   %acc
   SRT1(i).accdata = csvread([filelo,'computer
3\SR',num2str(i),'\tamping\11_03_Accel.csv'],1,2);
   SRT1(i).acc(:,2:4) = bsxfun(@minus, SRT1(i).accdata(:,1:3), SRT1(i).accdata(1,1:3));
   SRT1(i).acc(:,2:4) =
highpass(SRT1(i).acc(:,2:4),0.1,'Steepness',0.85,'StopbandAttenuation',60);
   SRT1(i).acc(:,5) = ( SRT1(i).acc(:,2).^2 + SRT1(i).acc(:,3).^2 ).^0.5;%horizontal acc value
   SRT1(i).acc(:,6) = ( SRT1(i).acc(:,2).^2 + SRT1(i).acc(:,3).^2 + SRT1(i).acc(:,4).^2
).^0.5;%all acc value



   h = 13;m = 28;
   for j = 1:length(SRT1(i).accdata(:,1))
      if j == 1
         SRT1(i).acc(j,1) = SRT1(i).accdata(j,9)/1000 + SRT1(i).accdata(j,8)+
(SRT1(i).accdata(j,7) - m) * 60 + (SRT1(i).accdata(j,6) - h) * 3600;
      else
         SRT1(i).acc(j,1) = (SRT1(i).accdata(j,9) - SRT1(i).accdata(j-1,9))/1000 +
SRT1(i).accdata(j,8) - SRT1(i).accdata(j-1,8) + (SRT1(i).accdata(j,7) - SRT1(i).accdata(j-1,7)) *
60 + (SRT1(i).accdata(j,6) - SRT1(i).accdata(j-1,6)) * 3600 + SRT1(i).acc(j-1,1);
      end
   end
   SRT1(i).acc(:,1) = SRT1(i).acc(:,1) - SRT1(i).acc(1,1);
   [SRT1(i).reacc(:,2:4),SRT1(i).reacc(:,1)] = resample(SRT1(i).acc(:,2:4),SRT1(i).acc(:,1),100);
   SRT1(i).reacc(:,5) = ( SRT1(i).reacc(:,2).^2 + SRT1(i).reacc(:,3).^2 ).^0.5;%horizontal acc
value
   SRT1(i).reacc(:,6) = ( SRT1(i).reacc(:,2).^2 + SRT1(i).reacc(:,3).^2 + SRT1(i).reacc(:,4).^2
).^0.5;%all acc value
```

```
   %eul
   SRT1(i).quat = csvread([filelo,'computer
3\SR',num2str(i),'\tamping\11_03_Quaternion.csv'],1,2);
   SRT1(i).eul(:,2:4) = quat2eul(SRT1(i).quat(:,1:4));
   SRT1(i).eul(:,2:4) = bsxfun(@minus, SRT1(i).eul(:,2:4), SRT1(i).eul(1,2:4));
   SRT1(i).eul(:,2:4) = bsxfun(@times, SRT1(i).eul(:,2:4), 180/pi);
   for j = 1:length(SRT1(i).quat(:,1))
      if j == 1
         SRT1(i).eul(j,1) = SRT1(i).quat(j,10)/1000 + SRT1(i).quat(j,9)+ (SRT1(i).quat(j,8) - m)
* 60 + (SRT1(i).quat(j,7) - h) * 3600;
      else
         SRT1(i).eul(j,1) = (SRT1(i).quat(j,10) - SRT1(i).quat(j-1,10))/1000 + SRT1(i).quat(j,9) -
SRT1(i).quat(j-1,9) + (SRT1(i).quat(j,8) - SRT1(i).quat(j-1,8)) * 60 + (SRT1(i).quat(j,7) -
SRT1(i).quat(j-1,7)) * 3600 + SRT1(i).eul(j-1,1);
      end
   end
   SRT1(i).eul(:,1) = SRT1(i).eul(:,1) - SRT1(i).eul(1,1);
   [SRT1(i).reeul(:,2:4),SRT1(i).reeul(:,1)] = resample(SRT1(i).eul(:,2:4),SRT1(i).eul(:,1),100);


   %pressure
   SRT1(i).voltage = csvread([filelo,'computer
3\SR',num2str(i),'\tamping\11_03_Pressure.csv'],1,2);
   SRcoff1{i} = csvread([filelo,'computer 3\SR',num2str(i),'\params.csv'],1,1);


   initvoltage(1) = mean(SRT1(i).voltage(1:100,1));
   initvoltage(2) = mean(SRT1(i).voltage(1:100,2));
   initvoltage(3) = mean(SRT1(i).voltage(1:100,3));


   SRT1(i).pressure(:,2) = (initvoltage(1) - SRT1(i).voltage(:,1)) .* SRcoff1{i}(2,1);% -
SRcoff1{i}(2,2) .* log(25) + SRcoff1{i}(2,3);
   SRT1(i).pressure(:,3) = (initvoltage(2) - SRT1(i).voltage(:,2)) .* SRcoff1{i}(3,1);% -
SRcoff1{i}(3,2) .* log(25) + SRcoff1{i}(3,3);
   SRT1(i).pressure(:,4) = (initvoltage(3) - SRT1(i).voltage(:,3)) .* SRcoff1{i}(1,1);% -
SRcoff1{i}(1,2) .* log(25) + SRcoff1{i}(1,3);
```

```
   SRT1(i).pressure(:,5) = SRT1(i).pressure(:,2) + SRT1(i).pressure(:,3) + SRT1(i).pressure(:,4);


   for j = 1:length(SRT1(i).voltage(:,1))
     if j == 1
        SRT1(i).pressure(j,1) = SRT1(i).voltage(j,9)/1000 + SRT1(i).voltage(j,8)+
(SRT1(i).voltage(j,7) - m) * 60 + (SRT1(i).voltage(j,6) - h) * 3600;
     else
        SRT1(i).pressure(j,1) = (SRT1(i).voltage(j,9) - SRT1(i).voltage(j-1,9))/1000 +
SRT1(i).voltage(j,8) - SRT1(i).voltage(j-1,8) + (SRT1(i).voltage(j,7) - SRT1(i).voltage(j-1,7)) *
60 + (SRT1(i).voltage(j,6) - SRT1(i).voltage(j-1,6)) * 3600 + SRT1(i).pressure(j-1,1);
     end
   end
   SRT1(i).pressure(:,1) = SRT1(i).pressure(:,1) - SRT1(i).pressure(1,1);
   [SRT1(i).repressure(:,2:4),SRT1(i).repressure(:,1)] =
resample(SRT1(i).pressure(:,2:4),SRT1(i).pressure(:,1),100);
   SRT1(i).repressure(:,5) = SRT1(i).repressure(:,2) + SRT1(i).repressure(:,3) +
SRT1(i).repressure(:,4);
end


%% com4
for i = 20 : 23
   SRT1(i).label = '1inst 0.6s';
   %acc
   SRT1(i).accdata = csvread([filelo,'computer
4\SR',num2str(i),'\tamping\11_03_Accel.csv'],1,2);
   SRT1(i).acc(:,2:4) = bsxfun(@minus, SRT1(i).accdata(:,1:3), SRT1(i).accdata(1,1:3));
   SRT1(i).acc(:,2:4) =
highpass(SRT1(i).acc(:,2:4),0.1,'Steepness',0.85,'StopbandAttenuation',60);
   SRT1(i).acc(:,5) = ( SRT1(i).acc(:,2).^2 + SRT1(i).acc(:,3).^2 ).^0.5;%horizontal acc value
   SRT1(i).acc(:,6) = ( SRT1(i).acc(:,2).^2 + SRT1(i).acc(:,3).^2 + SRT1(i).acc(:,4).^2
).^0.5;%all acc value



   h = 13;m = 26;
```

```
    for j = 1:length(SRT1(i).accdata(:,1))
        if j == 1
            SRT1(i).acc(j,1) = SRT1(i).accdata(j,9)/1000 + SRT1(i).accdata(j,8)+
(SRT1(i).accdata(j,7) - m) * 60 + (SRT1(i).accdata(j,6) - h) * 3600;
        else
            SRT1(i).acc(j,1) = (SRT1(i).accdata(j,9) - SRT1(i).accdata(j-1,9))/1000 +
SRT1(i).accdata(j,8) - SRT1(i).accdata(j-1,8) + (SRT1(i).accdata(j,7) - SRT1(i).accdata(j-1,7)) *
60 + (SRT1(i).accdata(j,6) - SRT1(i).accdata(j-1,6)) * 3600 + SRT1(i).acc(j-1,1);
        end
    end
    SRT1(i).acc(:,1) = SRT1(i).acc(:,1) - SRT1(i).acc(1,1);
    [SRT1(i).reacc(:,2:4),SRT1(i).reacc(:,1)] = resample(SRT1(i).acc(:,2:4),SRT1(i).acc(:,1),100);
    SRT1(i).reacc(:,5) = ( SRT1(i).reacc(:,2).^2 + SRT1(i).reacc(:,3).^2 ).^0.5;%horizontal acc
value
    SRT1(i).reacc(:,6) = ( SRT1(i).reacc(:,2).^2 + SRT1(i).reacc(:,3).^2 + SRT1(i).reacc(:,4).^2
).^0.5;%all acc value


    %eul
    SRT1(i).quat = csvread([filelo,'computer
4\SR',num2str(i),'\tamping\11_03_Quaternion.csv'],1,2);
    SRT1(i).eul(:,2:4) = quat2eul(SRT1(i).quat(:,1:4));
    SRT1(i).eul(:,2:4) = bsxfun(@minus, SRT1(i).eul(:,2:4), SRT1(i).eul(1,2:4));
    SRT1(i).eul(:,2:4) = bsxfun(@times, SRT1(i).eul(:,2:4), 180/pi);
    for j = 1:length(SRT1(i).quat(:,1))
        if j == 1
            SRT1(i).eul(j,1) = SRT1(i).quat(j,10)/1000 + SRT1(i).quat(j,9)+ (SRT1(i).quat(j,8) - m)
* 60 + (SRT1(i).quat(j,7) - h) * 3600;
        else
            SRT1(i).eul(j,1) = (SRT1(i).quat(j,10) - SRT1(i).quat(j-1,10))/1000 + SRT1(i).quat(j,9) -
SRT1(i).quat(j-1,9) + (SRT1(i).quat(j,8) - SRT1(i).quat(j-1,8)) * 60 + (SRT1(i).quat(j,7) -
SRT1(i).quat(j-1,7)) * 3600 + SRT1(i).eul(j-1,1);
        end
    end
    SRT1(i).eul(:,1) = SRT1(i).eul(:,1) - SRT1(i).eul(1,1);
    [SRT1(i).reeul(:,2:4),SRT1(i).reeul(:,1)] = resample(SRT1(i).eul(:,2:4),SRT1(i).eul(:,1),100);
```

```
   %pressure
   SRT1(i).voltage = csvread([filelo,'computer
4\SR',num2str(i),'\tamping\11_03_Pressure.csv'],1,2);
   SRcoff1{i} = csvread([filelo,'computer 4\SR',num2str(i),'\params.csv'],1,1);


   initvoltage(1) = mean(SRT1(i).voltage(1:100,1));
   initvoltage(2) = mean(SRT1(i).voltage(1:100,2));
   initvoltage(3) = mean(SRT1(i).voltage(1:100,3));


   SRT1(i).pressure(:,2) = (initvoltage(1) - SRT1(i).voltage(:,1)) .* SRcoff1{i}(2,1);% -
SRcoff1{i}(2,2) .* log(25) + SRcoff1{i}(2,3);
   SRT1(i).pressure(:,3) = (initvoltage(2) - SRT1(i).voltage(:,2)) .* SRcoff1{i}(3,1);% -
SRcoff1{i}(3,2) .* log(25) + SRcoff1{i}(3,3);
   SRT1(i).pressure(:,4) = (initvoltage(3) - SRT1(i).voltage(:,3)) .* SRcoff1{i}(1,1);% -
SRcoff1{i}(1,2) .* log(25) + SRcoff1{i}(1,3);
   SRT1(i).pressure(:,5) = SRT1(i).pressure(:,2) + SRT1(i).pressure(:,3) + SRT1(i).pressure(:,4);


   for j = 1:length(SRT1(i).voltage(:,1))
     if j == 1
        SRT1(i).pressure(j,1) = SRT1(i).voltage(j,9)/1000 + SRT1(i).voltage(j,8)+
(SRT1(i).voltage(j,7) - m) * 60 + (SRT1(i).voltage(j,6) - h) * 3600;
     else
        SRT1(i).pressure(j,1) = (SRT1(i).voltage(j,9) - SRT1(i).voltage(j-1,9))/1000 +
SRT1(i).voltage(j,8) - SRT1(i).voltage(j-1,8) + (SRT1(i).voltage(j,7) - SRT1(i).voltage(j-1,7)) *
60 + (SRT1(i).voltage(j,6) - SRT1(i).voltage(j-1,6)) * 3600 + SRT1(i).pressure(j-1,1);
     end
   end
   SRT1(i).pressure(:,1) = SRT1(i).pressure(:,1) - SRT1(i).pressure(1,1);
   [SRT1(i).repressure(:,2:4),SRT1(i).repressure(:,1)] =
resample(SRT1(i).pressure(:,2:4),SRT1(i).pressure(:,1),100);
   SRT1(i).repressure(:,5) = SRT1(i).repressure(:,2) + SRT1(i).repressure(:,3) +
SRT1(i).repressure(:,4);
end
toc
```

Abbreviations and Acronyms

ACRONYM	DEFINITION
FRA	Federal Railroad Administration
NS	Norfolk Southern
DAQ	Data Acquisition
GMT	gross million tonnes
IQR	interquartile range